

RESEARCH ARTICLE



# Predicting transdermal fentanyl delivery using physics-based simulations for tailored therapy based on the age

Flora Bahrami<sup>a,b</sup>, René Michel Rossi<sup>a</sup> and Thijs Defraeye<sup>a</sup>

<sup>a</sup>Empa, Swiss Federal Laboratories for Materials Science and Technology, Laboratory for Biomimetic Membranes and Textiles, St. Gallen, Switzerland; <sup>b</sup>ARTORG Center for Biomedical Engineering Research, University of Bern, Bern, Switzerland

## ABSTRACT

Transdermal fentanyl patches are an effective alternative to the sustained release of oral morphine for chronic pain management. Due to the narrow therapeutic range of fentanyl, the concentration of fentanyl in the blood needs to be carefully monitored. Only then can effective pain relief be achieved while avoiding adverse effects such as respiratory depression. This study developed a physics-based digital twin of a patient by implementing drug uptake, pharmacokinetics, and pharmacodynamics models. The twin was employed to predict the *in-silico* effect of conventional fentanyl transdermal in a 20–80-year-old virtual patient. The results show that, with increasing age, the maximum transdermal fentanyl flux and maximum concentration of fentanyl in the blood decreased by 11.4% and 7.0%, respectively. However, the results also show that as the patient's age increases, the pain relief increases by 45.2%. Furthermore, the digital twin was used to propose a tailored therapy based on the patient's age. This predesigned therapy customized the duration of applying the commercialized fentanyl patches. According to this therapy, a 20-year-old patient needs to change the patch 2.1 times more frequently than conventional therapy, which leads to 30% more pain relief and 315% more time without pain. In addition, the digital twin was updated by the patient's pain intensity feedback. Such therapy increased the patient's breathing rate while providing effective pain relief, so a safer treatment. We quantified the added value of a patient's physics-based digital twin and sketched the future roadmap for implementing such twin-assisted treatment into the clinics.



**Nomenclature:**  $c_i$ : The concentration of fentanyl in layer  $i$  (in the drug uptake model) [ $\text{ng ml}^{-1}$ ];  $c_p$ : The concentration of fentanyl in the central compartment [ $\text{ng ml}^{-1}$ ];  $c_r$ : The concentration of fentanyl in the rapid equilibrated compartment [ $\text{ng ml}^{-1}$ ];  $c_s$ : The concentration of fentanyl in the slow equilibrated compartment [ $\text{ng ml}^{-1}$ ];  $c_g$ : The concentration of fentanyl in the gastrointestinal compartment [ $\text{ng ml}^{-1}$ ];  $c_l$ : The concentration of fentanyl in the hepatic compartment [ $\text{ng ml}^{-1}$ ];  $c_e$ : The concentration of fentanyl in the effect compartment [ $\text{ng ml}^{-1}$ ];  $D_i$ : Diffusion coefficient of fentanyl in layer  $i$  (in the mechanistic model) [ $\text{m}^2 \text{s}^{-1}$ ];  $D_0$ : Base diffusion coefficient of fentanyl [ $\text{m}^2 \text{s}^{-1}$ ];  $D_T$ : Diffusion coefficient of fentanyl at temperature  $T$  [ $\text{m}^2 \text{s}^{-1}$ ];  $D_{306}$ : Diffusion coefficient of fentanyl at 306[K] [ $\text{m}^2 \text{s}^{-1}$ ];  $d_{pt}$ : The thickness of the transdermal patch [ $\mu\text{m}$ ];  $d_{sc}$ : The thickness of the stratum corneum [ $\mu\text{m}$ ];  $d_{vep}$ : The thickness of the viable epidermis [ $\mu\text{m}$ ];  $d_{edm}$ : The thickness of the equivalent dermis [ $\mu\text{m}$ ];  $E_i$ : The intensity of effect  $i$ ;  $E_i^0$ : The baseline of effect  $i$ ;  $E_i^{max}$ : The maximum effect  $i$ ;  $EC_{50,i}$ : The concentration related to half-maximum effect  $i$  [ $\text{ng ml}^{-1}$ ];  $f_u$ : The fraction of unbound fentanyl in plasma;  $j$ : Fentanyl flux in layer  $i$  (in the mechanistic model);  $K_{ij}$ : The partition coefficient of fentanyl between layer  $i$  to  $j$  (in the mechanistic model);  $K_i$ : The drug capacity in layer  $i$  (in the mechanistic model);  $k_{cs}$ : Inter-compartmental first-order equilibrium rate constant (central to slow equilibrated) [ $\text{min}^{-1}$ ];  $k_{cr}$ : Inter-compartmental first-order equilibrium rate constant (central to rapid equilibrated) [ $\text{min}^{-1}$ ];  $k_{cg}$ : Inter-compartmental first-order equilibrium rate constant (central to gastrointestinal) [ $\text{min}^{-1}$ ];  $k_{ch}$ : Inter-compartmental first-order equilibrium rate constant (central to hepatic) [ $\text{min}^{-1}$ ];  $k_{sc}$ : Inter-compartmental first-order equilibrium rate constant (slow equilibrated to central) [ $\text{min}^{-1}$ ];  $k_{rc}$ : Inter-compartmental first-order equilibrium rate constant (rapid equilibrated to central) [ $\text{min}^{-1}$ ];  $k_{hc}$ : Inter-compartmental first-order equilibrium rate constant (hepatic to central) [ $\text{min}^{-1}$ ];  $k_{gh}$ : Inter-compartmental first-order equilibrium rate constant (gastrointestinal to hepatic) [ $\text{min}^{-1}$ ];  $k_{met}$ : Metabolization rate constant [ $\text{min}^{-1}$ ];  $k_{re}$ : Renal clearance rate constant [ $\text{min}^{-1}$ ];  $k_e$ : Inter-compartmental first-order equilibrium rate constant (for effect compartment) [ $\text{min}^{-1}$ ];  $S$ : Sensitivity index;  $t$ : Time [h];  $t_D$ : Time lag [h];  $U_x$ : Dependent variable related to  $x_i$  for sensitivity analysis;  $V_c$ : The apparent volume of the central compartment [L];  $V_s$ : The apparent volume of the slow equilibrated compartment [L];  $V_r$ : The apparent volume of the rapid equilibrated compartment [L];  $V_g$ : The apparent volume of the gastrointestinal compartment [L];  $V_h$ : The apparent volume of the hepatic compartment [L];  $x_i$ : The independent variable which sensitivity analysis is done based on it;  $\gamma$ : Hill coefficient;  $\psi_i$ : Drug potential in domain  $i$  [ $\text{ng ml}^{-1}$ ]


## ARTICLE HISTORY

Received 6 January 2022  
Revised 22 February 2022  
Accepted 2 March 2022

## KEYWORDS

Tailored therapy; pharmacology; *in-silico* modeling; pain management; mechanistic modeling

**CONTACT** Thijs Defraeye,  [thijs.defraeye@empa.ch](mailto:thijs.defraeye@empa.ch)  Empa, Swiss Federal Laboratories for Materials Science and Technology, Laboratory for Biomimetic Membranes and Textiles, Lerchenfeldstrasse 5, St. Gallen, CH-9014, Switzerland

 Supplemental data for this article is available online at <https://doi.org/10.1080/10717544.2022.2050846>.

© 2022 The Author(s). Published by Informa UK Limited, trading as Taylor & Francis Group.

This is an Open Access article distributed under the terms of the Creative Commons Attribution License (<http://creativecommons.org/licenses/by/4.0/>), which permits unrestricted use, distribution, and reproduction in any medium, provided the original work is properly cited.

## 1. Introduction

Severe chronic pain is a frequent symptom in cancer patients, and about 70–80% of the patients in advanced cancer stages deal with such pain (Caraceni et al., 2012). However, proper pain treatment is challenging, considering the complex nature of pain and differentiated actions of opioids (Andresen et al., 2011). Untreated or poorly-treated pain could be overwhelming for the patients and reduce their quality of life (Serlin et al., 1995). Fentanyl is clinically used to treat moderate-to-severe cancer pain. Fentanyl is a synthetic opioid that is used in cases where non-steroidal anti-inflammatory drugs (NSAIDs) are insufficient (Orsini et al., 2006). As an alternative to oral and parenteral delivery, transdermal fentanyl delivery (TDD) is a clinically-approved therapy, which is successful due to its low molecular weight, high potency, and lipid solubility of fentanyl. The key advantage of transdermal fentanyl delivery, besides simplicity and noninvasive delivery, is that it offers a controlled delivery of fentanyl and avoids the first-pass metabolism (Muijsers and Wagstaff, 2001; Marier et al., 2006).

Transdermal fentanyl therapy shows high inter-individual and intra-individual variability (Lennernäs et al., 2005; Kuip et al., 2017; Geist et al., 2019). Several factors can cause these variabilities (Kuip et al., 2017), including a different clearance rate (Grond et al., 2000), amongst others. Additionally, fentanyl has a narrow therapeutic range. Alongside the analgesic effect, fentanyl affects the ventilation rate in patients and could cause respiratory depression, which, in severe cases, could lead to patient death (Yassen et al., 2008). By considering these side effects, it is important to keep the fentanyl concentration in the blood at such a level that sufficient analgesia is reached while avoiding adverse effects such as respiratory depression for each patient. The conventional therapy for using the transdermal fentanyl patch, which is being used in clinics, is applying a transdermal patch for 72 hours on the skin (US Food and Drug Administration, “Duragesic Label”, 2005; Kuip et al., 2018). Applying a similar therapy for all the patients, ignoring the physiological states and differences in the therapeutic range for each patient, often fails to treat the pain effectively (Breitbart et al., 2000). In order to determine the suitable fentanyl patch, prior to applying the patch, the patient will receive oral morphine. This practice involves a trial-and-error approach where the oral dose of morphine is gradually increased while carefully monitoring the patient’s response until an individualized dosage and therapy are reached. With the advent of physics-based simulations of drug delivery processes, truly individualized therapies can be achieved (Corral-Acero et al., 2020).

Mechanistic, first-principles-based modeling and simulation of transdermal drug delivery systems (TDDs) are usually done using two approaches. The first approach is the simulation of the drug’s penetration process through the skin layers, especially the stratum corneum at different scales. In this approach, at the nano-scale, the penetration of drugs in lipid bilayers of the stratum corneum (SC) is modeled by using molecular dynamics simulation (Gupta and Rai, 2018;

Lundborg et al., 2018; Van der Paal et al., 2019). One of the results of this set of simulations is the diffusion coefficient for transient diffusion of the drug in the modeled layer (Yang et al., 2018; Ruan et al., 2019). At the meso- and micro-scale, brick-and-mortar and cellular models of the SC are employed to model the drug transport (Naegel et al., 2013; Chen et al., 2016; Walicka and Iwanowska-Chomiak, 2018). Fickian diffusion-based models are typically used at the macro-scale to obtain drug penetration through the skin into the blood circulation system (Manitz et al., 1998; Anissimov et al., 2013; Weiser and Saltzman, 2014). Such models can accurately capture the time-lag caused by the skin between the drug release and the drug uptake. Pharmacokinetic (PK) and pharmacodynamic (PD) modeling and simulation are performed in the second approach. In this approach, the skin is modeled as a depot to obtain the incoming flux of drugs to the blood circulation system (Nelson and Schwaner, 2009; Heikkinen et al., 2015). The PK model calculates the concentration of drug in the plasma, and the PD model provides the drug effect(s) related to the plasma concentration of the drug (Björkman, 2003; Obara and Egan, 2013; Li et al., 2017; Madden et al., 2019; Pan and Duffull, 2019). To propose a successful transdermal therapy *in-silico*, however, both the delayed drug uptake kinetics through the skin and the fate of the drug in the human body must be predicted *in-silico*. To our best knowledge, such a complete mechanistic model that follows the drug from the transdermal patch until the organ where it evokes pain relief has not been set up. In addition, by connecting the model to the real-world patient via patient physiology and pain feedback, a so-called digital twin of the patient for fentanyl delivery can be created to personalize therapy. Such a connection can be established by tailoring the digital twin to a certain patient or a certain class of patients (e.g. age group). More advanced digital twins are created by establishing real-time feedback of the patient to the twin, for example, the experienced pain scale or sensed biomarkers. Implementing digital twins in healthcare enables *in silico* trials on a population of virtual patients (Defraeye et al., 2020a; Sinisi et al., 2020), and there were studies on the deployment of digital twins for training surgeons through interactive virtual simulations (Dequidt et al., 2013) or digital twins for aerosol pulmonary drug therapy (Feng et al., 2018; 2018). However, the digital twin concept is still novel, and its full potential has not been exploited so far, including for transdermal drug delivery.

In this study, we developed a physics-based digital twin for a virtual patient that takes into account the drug diffusion from the transdermal patch through the skin layers to reach the blood circulation. The twin further includes PK and PD models in order to monitor the fate of fentanyl and its impact on pain sensation, and it is linked to virtual patient feedback. This digital twin is tailored based on the virtual patient’s age and proposes a modified therapy for the virtual patient based on the calculated pain relief, age, and patient feedback. This paper quantifies the added value of such physics-based digital twins for effective pain management for patients. This is a step toward tailored fentanyl

transdermal therapy based on the patient's physiological features. In the developed digital twin, the PK model was validated, the PD model was calibrated based on the literature, and the uptake model was validated in our previous study (Defraeye et al., 2020b). By using these digital twins, in a first step, we studied the effect of age on the outcome of the same fentanyl transdermal therapy. In the second step, we controlled the incoming flux of drugs to the body for the virtual patient at different ages in a way to have sufficient pain relief while avoiding hypoventilation. Finally, real-time feedback connected the digital twin to the virtual patient to modify the pre-designed therapy based on the virtual patient's need.

## 2. Materials and methods

### 2.1. Mechanistic multiphysics model for transdermal drug delivery

The developed physics-based digital twin in this study consisted of 3 model blocks to simulate transdermal drug uptake, PK, and PD models. In the transdermal drug uptake model, the flux of fentanyl from the patch through the skin into the blood circulation system was calculated. The PK model calculated fentanyl distribution through the body, metabolism in the liver, and elimination by the kidneys. The result of the PK model is the plasma fentanyl concentration versus time. In the PD model, the fentanyl concentration in the effect compartment was calculated. Based on this concentration, pain relief and ventilation rate as the effects of fentanyl were obtained. The overall structure of this physics-based digital twin is shown in Figure 1.

### 2.1.1. Transdermal drug uptake in skin

**2.1.1.1. Computational system configuration.** A mechanistic continuum model was built in order to simulate fentanyl release from a transdermal patch, diffusion through the skin, and uptake by blood circulation. Based on fentanyl properties, such as high lipophilicity and low molecular weight, fentanyl is suitable to be used via the first generation of transdermal patches. In a way, the penetration of fentanyl through the skin barrier is diffusion-driven (Marier et al., 2006), and there is no need for penetration enhancers. The model and simulation were built and executed according to best practice guidelines (or clinical practice guidelines) in modeling for medical device design (Casey and Wintergerste, 2000; FDA, 2016).

The geometry of the drug uptake model and boundary conditions are shown in Figure 2. The system configuration consists of four blocks with a square surface area representing fentanyl patch, stratum corneum, viable epidermis, and a part of the dermis. Transdermal patches are designed to deliver the drug at an approximately constant rate (Chien and Lin, 2007). Therefore, the fentanyl patches are commercially labeled with a targeted drug release rate of 12–100  $\mu\text{g h}^{-1}$ , which is the average rate over 72 h (Muijsers and Wagstaff, 2001).

We chose the patch's size based on a Duragesic® fentanyl patch with a nominal flux of 75  $\mu\text{g h}^{-1}$ , which contains 12.6 mg of fentanyl (US Food and Drug Administration, "Duragesic Label", 2005). The patch's surface area is 30  $\text{cm}^2$ , and the thickness of the patch was considered 50.8  $\mu\text{m}$ . Here, we used the diffusion parameters for the transdermal patch and epidermis layer (stratum corneum and viable epidermis) from our previous study (Defraeye et al., 2020b,

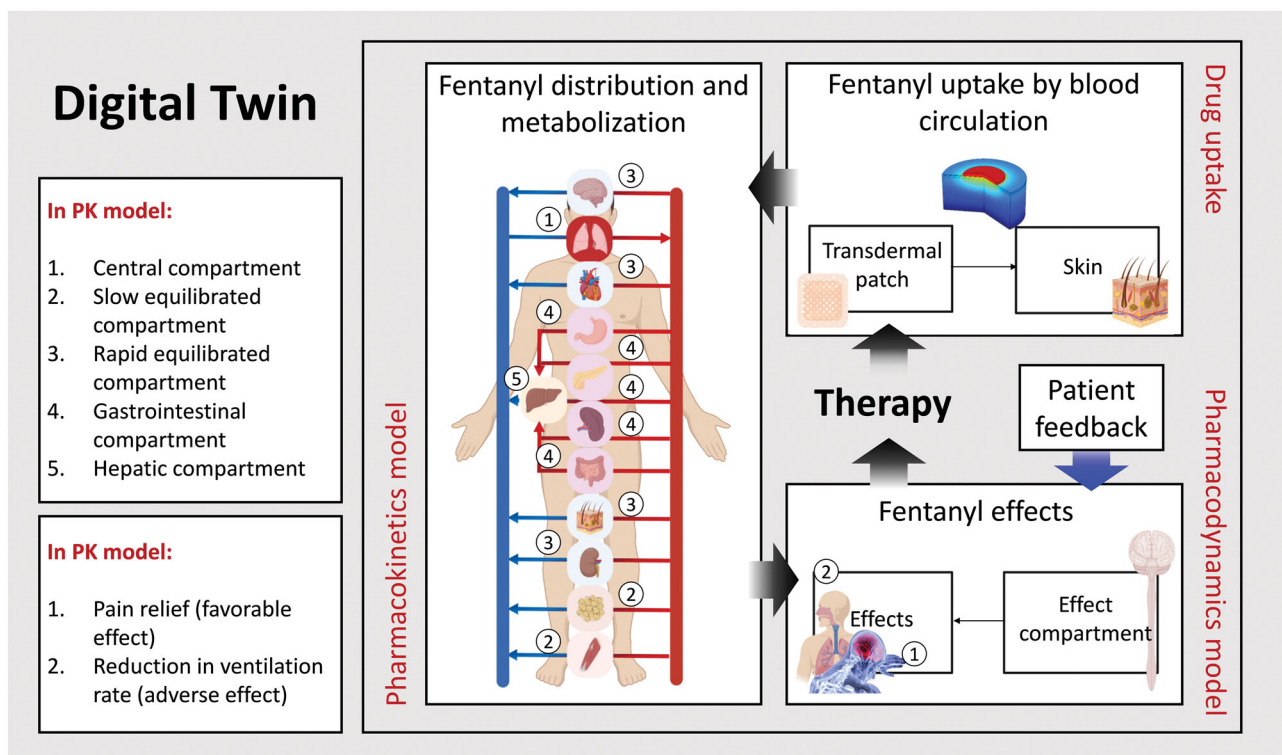


Figure 1. The overall structure of an implemented digital twin for transdermal fentanyl therapy (Created with BioRender.com).

2021). In that study, the model parameters' values were optimized to reach the best match with experimental data, where the epidermis was considered a single layer. The value of these parameters is mentioned in section Material properties and transport characteristics of skin and patch, Table 1.

Due to the presence of capillary vessels in the dermis, the drug would be uptaken by the vessels after the penetration of the drug from the epidermis. These vessels are in different depths in the dermis, and the drug uptake happens in various lengths of the dermis. In this study, we assumed that the drug was transferred through the dermis only by the diffusion process, which is a simplified assumption. If we consider the whole length of the dermis by only applying the diffusion process, the time lag increases up to 11 h (refer to Equation 5, section Governing equations), which is considerably different from reported values (1–2 h time-lag (Jeal and Benfield, 1997)). In the real situation, due to plasma flow into and out of the vessels, there is an advection mechanism as well. As a result, the drug penetration mechanism in the dermis is a combination of diffusion and advection. However, to modify this assumption, instead of modeling the dermis's whole thickness, we considered an equivalent diffusive length of the dermis. The dermis's equivalent length was obtained based on the reported experimental data of time-lag for detecting fentanyl in the plasma (Jeal and Benfield, 1997) and the diffusion coefficient of fentanyl in the dermis.

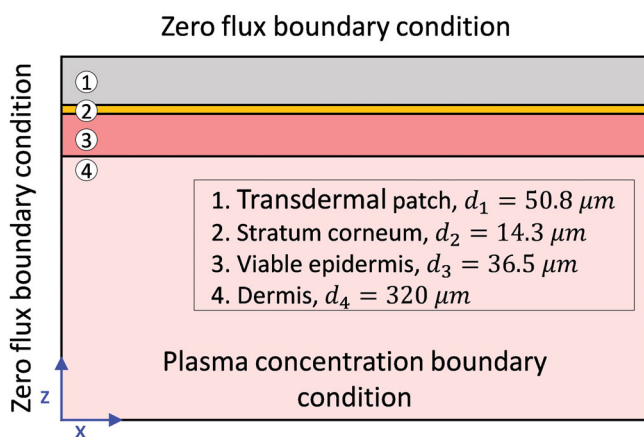


Figure 2. Geometrical model of the transdermal patch and skin layers.

**2.1.1.2. Governing equations.** The transport of fentanyl in the patch and skin was modeled by one-dimensional transient diffusion. The fentanyl concentration in the patch and skin layers is denoted by  $c_i(z, t)$  [ $\text{kg m}^{-3}$ ]. This diffusion process is described by Fick's second law, which is mentioned in Equation 1 (Manitz et al., 1998).

$$\frac{\partial c_i}{\partial t} = -\nabla \cdot (J_i) = \nabla \cdot (D_i \nabla c_i) \tag{1}$$

where  $J_i$  and  $D_i$  are the flux [ $\text{kg m}^{-2} \text{s}^{-1}$ ] and diffusion coefficient [ $\text{m}^2 \text{s}^{-1}$ ] of fentanyl in domain  $i$ , respectively. At the interface of two layers (patch and skin layers), due to the different solubility of drugs in different layers, partitioning should be considered. The partition coefficient at the interface is defined in Equation 2 (Manitz et al., 1998).

$$c_i(z, t) = K_{ijj} c_j(z, t) \tag{2}$$

Here,  $K_{ijj}$  is the partition coefficient of fentanyl from domain  $i$  to domain  $j$ . As a result of partitioning, a discontinuity will occur at the interface, which is inconvenient to solve computationally. To avoid this problem, another variable was defined, which is continuous throughout the whole domain. The relation of this new variable  $\psi_i$  and  $c_i$  is mentioned in Equation 3.

$$c_i(z, t) = K_i \psi_i(z, t) \tag{3}$$

In this equation,  $K_i$  and  $\psi_i$  are drug capacity and drug potential in domain  $i$ . As mentioned before, we assumed that  $\psi_i$  is continuous; therefore, at the interface, the drug potential in domain  $i$  and  $j$  are equal. By applying this condition in Equations 2 and 3, we arrive at Equation 4.

$$K_{ijj} = \frac{K_i}{K_j} \tag{4}$$

The equivalent length of the dermis was considered based on the time lag of detection of fentanyl after applying the patch on the skin. Between the application of the first fentanyl patch ( $100$  or  $75 \mu\text{g h}^{-1}$ ) and detection of fentanyl in blood circulation ( $> 0.1 \text{ ng ml}^{-1}$ ), there is a 1–2 h time-lag (Jeal and Benfield, 1997). Based on the reported range, we considered the time-lag as 1.5 [h]. Both epidermis and dermis play a role in this delay. We calculated the time lag caused by the epidermis by using the mechanistic model. After subsiding the delay caused by the epidermis, the dermis was responsible for the remaining part. By using Equation 5, the equivalent diffusive length of the dermis was obtained.

Table 1. Parameters involved in the mechanistic model for 20 years old virtual patient.

Parameter	Description	Symbol	Value	References
Thickness	Patch (reservoir and membrane)	$d_{pt}$	$50.8 \mu\text{m}$	Rim et al., 2005
	Stratum corneum	$d_{sc}$	$14.3 \mu\text{m}$	(modified) Boireau-Adamezyk et al., 2014
	Viable epidermis	$d_{vep}$	$36.5 \mu\text{m}$	Rim et al., 2005
	Equivalent dermis	$d_{Edm}$	$320 \mu\text{m}$	(modified) Robert and Robert, 2009
Diffusion coefficient	Patch	$D_{pt}$	$6.91 \times 10^{-16} \text{ m}^2 \text{ s}^{-1}$	Defraeye et al., 2021
	Epidermis	$D_{ep}$	$3.00 \times 10^{-14} \text{ m}^2 \text{ s}^{-1}$	Defraeye et al., 2020c
	Dermis	$D_{dm}$	$3.82 \times 10^{-11} \text{ m}^2 \text{ s}^{-1}$	Karin Homber et al., 2008
Partition coefficient	Patch	$K_{pt/ep}$	$1/3.4 = 0.29$	Defraeye et al., 2021
	Epidermis	$K_{ep/dm}$	$3.4/3.4 = 1$	Defraeye et al., 2021
	Dermis	–	–	–
Drug capacity	Patch	$K_{pt}$	1	–
	Epidermis	$K_{ep}$	3.4	Defraeye et al., 2021
	Dermis	$K_{dm}$	3.4	–



$$t_D = \frac{d_{Edm}^2}{6 D_{dm}} \quad (5)$$

In this equation,  $t_D$  is the time lag [s] and  $d_{Edm}$  [m] is the equivalent length of the dermis (Berner and John, 1994). The diffusion coefficient of fentanyl in the dermis is shown by  $D_{dm}$  [ $\text{m}^2 \text{s}^{-1}$ ], which obtained by Equation 6.

$$D_{dm} = D_0 e^{\frac{-E}{RT}} + 400(D_T - D_{306}) \quad (6)$$

Which,  $D_0$  is the base diffusion coefficient,  $D_{306}$  is the diffusion coefficient at  $T = 306$  K, and  $D_T$  is the diffusion coefficient in operating temperature, which is 310.5 K (Karin Homber et al., 2008).

**2.1.1.3. Material properties and transport characteristics of skin and patch.** The drug used in this simulation is fentanyl, with a molecular weight of  $336.5 \text{ g mol}^{-1}$ . The material properties used in this study are mentioned in Table 1. In this study, we assumed the fentanyl capacity of the dermis to be the same as the epidermis. This assumption was made due to the lack of reported data in this situation.

**2.1.1.4. Boundary and initial conditions.** In this mechanistic model, the source of fentanyl is the transdermal patch, which has an initial concentration of  $80 \text{ kg m}^{-3}$ , equivalent to 12.6 mg of fentanyl. This amount of drug is based on the Duragesic® fentanyl patch with  $75 \mu\text{g h}^{-1}$  flux of drug. As the initial condition, it is assumed that there is no fentanyl in the skin layers. We assumed that there is no flux in peripheral boundaries, and the flux of the drug is vertical from the patch to the end of the dermis. At the bottom boundary of the dermis, the concentration is equal to the fentanyl concentration in blood circulation, which is zero at the beginning (the concentration of fentanyl in blood circulation is obtained by the PK model).

### 2.1.2. Physiologically-based pharmacokinetics modeling

The physiologically-based pharmacokinetics (PBPK) model was used to calculate the concentration of fentanyl in plasma by considering drug metabolization, elimination, and distribution through the body. The PK model was developed based on the physiology of the patient and the pharmacological mechanism of fentanyl. In PK modeling, it is common to lump different organs into a single functioning kinetic unit, despite the fact that they are anatomically distinct (Upton et al., 2016). To capture better the complexity of fentanyl transport in the human body and the resulting drug concentration in the blood plasma, five different kinetic compartments were used in the present study:

1. A central compartment, namely the blood circulation system and lungs (Equation 7).
2. A slowly equilibrating compartment, which includes muscles, carcass, and fat tissue (Equation 8).
3. A rapidly equilibrating compartment, which includes the brain, heart, skin, and kidneys (Equation 9)
4. A gastrointestinal compartment, which includes the spleen, gut, and pancreas. In this compartment, the

outcoming flow goes to the hepatic compartment instead of the central compartment (Equation 10).

5. A hepatic compartment, where the CYP metabolism of fentanyl is occurring. This is the main elimination route of fentanyl from the human body (Equation 11).

An overview of the PK model is given in Figure 1. To evaluate the concentration of fentanyl in each compartment, the law of conservation of mass by considering well-mixed compartments was applied. By using the first-order kinetic rate law, the fentanyl concentration at each compartment based on transferring drug between compartments, metabolization, and elimination was calculated. The ordinary differential equations related to mass conservation for each compartment are mentioned below:

$$\frac{\partial C_p}{\partial t} = Flux_d \frac{A}{V_c} - (k_{cs} + k_{cr} + k_{cl} + k_g - k_{re}) f_u C_p + k_{rc} C_r + k_{sc} C_s + k_{lc} C_l \quad (7)$$

$$\frac{\partial C_r}{\partial t} = k_{cr} C_p - k_{rc} C_r \quad (8)$$

$$\frac{\partial C_s}{\partial t} = k_{cs} C_p - k_{sc} C_s \quad (9)$$

$$\frac{\partial C_g}{\partial t} = k_{cg} C_p - k_{gl} C_g \quad (10)$$

$$\frac{\partial C_l}{\partial t} = k_{cl} C_p - k_{lc} C_l + k_{gl} C_g - k_{met} C_l \quad (11)$$

In this set of equations,  $C_p$ ,  $C_r$ ,  $C_s$ ,  $C_g$ , and  $C_l$  are concentration of fentanyl in central, rapid equilibrated, slow equilibrated, gastrointestinal and hepatic compartments, respectively.  $f_u$  is the unbound fraction of fentanyl in the central compartment.  $k_{ij}$ ,  $k_{met}$ , and  $k_{re}$  are the first-order equilibrium rate constants for inter-compartmental clearance, CYP metabolism, and renal clearance, respectively. In fentanyl therapy, the CYP metabolism is the main elimination way of fentanyl. Therefore, consuming fentanyl along with the CYP suppresser medicines such as ritonavir can lead to a high concentration of fentanyl in the plasma. Consequently, the use of ritonavir and fentanyl simultaneously needs to be done cautiously (Oikkola et al., 1999). The parameters used in these equations are specified in Table 2.

### 2.1.3. Mechanism-based pharmacodynamics model

In the PD model, the effects of fentanyl – pain relief and reduction of ventilation rate – were calculated. In fentanyl pharmacology, the drug effect will lag behind the fentanyl concentration in the plasma. As fentanyl rapidly binds to  $\mu$ -receptors in the central nervous system (CNS), the biophase distribution model can approximate the fentanyl concentration in the effect compartment based on plasma concentration (Yassen et al., 2007). The effect compartment is a theoretical concept that is assumed to have the same distributional properties as the drug's site of action (Wright et al., 2011). This effect compartment is used to describe the time course between plasma drug concentration and the effect (Algera et al., 2019). The biophase concentration of fentanyl

**Table 2.** Parameters involved in the pharmacokinetics model.

Parameter	Description	Symbol	Value	References	Note
The apparent volume of the compartment (for fentanyl)	Central compartment	$V_c$	23.8 L	Björkman, 2003	They are calculated based on the information in the literature.
	Slow equilibrated compartment	$V_s$	808 L		
	Rapid equilibrated compartment	$V_r$	24.5 L		
	Gastrointestinal compartment	$V_g$	17.3 L		
	Hepatic compartment	$V_l$	20.4 L		
Inter-compartmental first-order equilibrium rate constant	Central to slow equilibrated	$k_{cs}$	$1.5 \times 10^{-3} s^{-1}$	Björkman, 2003; Björkman et al., 1998	
	Central to rapid equilibrated	$k_{cr}$	$1.2 \times 10^{-3} s^{-1}$		
	Central to gastrointestinal	$k_{cg}$	$5 \times 10^{-4} s^{-1}$		
	Central to hepatic	$k_{ch}$	$1.2 \times 10^{-4} s^{-1}$		
	Slow equilibrated to central	$k_{sc}$	$5 \times 10^{-5} s^{-1}$		
	Rapid equilibrated to central	$k_{rc}$	$1.2 \times 10^{-3} s^{-1}$		
	Hepatic to central	$k_{hc}$	$7 \times 10^{-4} s^{-1}$		
Elimination of constant rate	Gastrointestinal to hepatic	$k_{gl}$	$5 \times 10^{-5} s^{-1}$	Encinas et al., 2013	
	Cyp metabolism	$k_{rmet}$	$4.2 \times 10^{-3} s^{-1}$		
	Renal clearance	$k_{re}$	$3 \times 10^{-5} s^{-1}$		
The unbound fraction of fentanyl	Central compartment	$f_u$	0.22	Miller et al., 1997	-

was obtained by using a standard effect-compartment equation (Equation 12).

$$\frac{\partial c_{e,i}}{\partial t} = k_{e,i} (c_p - c_{e,i}) \tag{12}$$

where  $c_{e,i}$  is the fentanyl concentration in the effect compartment,  $k_{e,i}$  is the first-order equilibrium rate constant, and  $i$  represents the effect (subscript Visual analog scale (VAS) for pain relief and subscript  $rd$  for reduction in ventilation rate). The values for parameters of the PD model are brought in Table 3.

**2.1.3.1 Drug effect.** Fentanyl molecules target opioid receptors, which are mainly located in the brain within specialized neuroanatomical structures, which control emotion, pain, and addictive properties. Activation of opioid receptors by fentanyl will produce analgesia (Ramos-Matos and Lopez-Ojeda, 2017). On the other hand, fentanyl activates opioid receptors on neurons within respiratory networks of the brainstem, which might lead to opioid-induced respiratory depression (Algera et al., 2019). However, respiratory depression does not occur for all patients under fentanyl transdermal therapy. Here we track the ventilation rate as a factor to evaluate the risk of respiratory depression. Medicines like naloxone can reverse the effect of opioids in order to reduce the risk of respiratory depression. Different studies show that naloxone is more successful for morphine compared to fentanyl (Hill et al., 2020). However, we still did not consider naloxone in this study, and we solely monitored the ventilation rate of the patient. Fentanyl therapy can cause other side effects such as nausea, vomiting, constipation, dry mouth, sleepiness, confusion, weakness, and sweating. However, most patients develop a tolerance toward the effects and side effects of fentanyl (US Food and Drug Administration, "Duragesic Label", 2005). Therefore, only respiratory depression, the life-threatening side effect, was considered in this study. In this study, the changes in ventilation rate (related to respiratory depression) and VAS pain score (to measure pain relief) were considered the main effects of fentanyl on the patient. A sigmoidal model based on the maximum

effect ( $E_{max}$ ) best describes the fentanyl effects related to pain relief and reduction of ventilation rate. Maximum effect ( $E_{max}$ ) represents the maximum possible deviation from the baseline effect. The baseline effect is the physiology state before using the drug, which in this case, the baseline effects are initial pain intensity and initial ventilation rate. The intensity of pharmacologic effects of fentanyl for pain relief and ventilation rate based on maximum effect, and Equation 13 calculates fentanyl concentration in effect compartments.

$$E_i = E_i^0 - E_i^{max} \left( \frac{c_{e,i}^{\gamma_i}}{EC_{50,i}^{\gamma_i} + c_{e,i}^{\gamma_i}} \right) \tag{13}$$

In Equation 13,  $E_i$ ,  $E_i^0$ , and  $E_i^{max}$  are the intensity of the pharmacologic, baseline, and maximum reachable effect, respectively. Here, the pharmacologic effect is the intensity of pain or minute ventilation of the patient. The baseline effect shows the state of pain or the patient's minute ventilation before the administration of the drug.  $EC_{50,i}$  is the concentration of drug in plasma which corresponds to half of the achievable effect of the drug. In this study,  $EC_{50,VAS}$  (for pain relief) is the concentration when the pain intensity reaches half of the initial pain intensity and  $EC_{50,rd}$  (for the reduction in ventilation rate) is the concentration when the ventilation rate reaches half of its initial rate, and  $\gamma_i$  is the Hill coefficient (Yassen et al., 2007).

The PD model parameters related to the reduction of ventilation rate were obtained from values reported in the literature (Yassen et al., 2007). The values used for these parameters are mentioned in Table 3. The corresponding values of the PD model for pain relief were obtained by fitting a sigmoidal model to experimental data from the literature (Sandler et al., 1992), and the calculated values are brought in Table 2. In modeling the VAS pain score, we assumed that the initial VAS pain score for all the virtual patients is equal to 7, which lies in the range of severe pain. Another assumption is that we considered the cause of the pain to be constant throughout the therapy. This assumption implies that if we remove the patch after the concentration of fentanyl reaches zero, the VAS pain score will return to its initial level.

**Table 3.** Parameters involved in the pharmacodynamics model for 20 years old virtual patient.

Effect	Parameter	Symbol	Value	References	Note
Ventilation rate	First-order equilibrium rate constant	$k_{e, rd}$	$7 \times 10^{-4} \text{ s}^{-1}$	Yassen et al., 2007	–
	Baseline effect	$E_{rd}^0$	$20 \text{ L min}^{-1}$		–
	Maximum effect	$E_{rd}^{max}$	$12 \times 0.91 \text{ L min}^{-1}$		–
	Half maximal effective concentration	$EC_{50, rd}$	$1.14 \text{ ng ml}^{-1}$		–
	Hill coefficient	$\gamma_{rd}$	2.68		–
VAS pain score	First-order equilibrium rate constant	$k_{e, VAS}^{**}$	$2 \times 10^{-3} \text{ s}^{-1}$	Encinas et al., 2013	–
	Baseline effect	$E_{VAS}^0$	7		–
	Maximum effect	$E_{VAS}^{max}$	7	–	–
	Half maximal effective concentration	$EC_{50, VAS}$	$1.35 \text{ ng ml}^{-1}$	Sandler et al., 1992	Calculated based on fitting of the information in the literature.
	Hill coefficient	$\gamma_{VAS}$	2.7		

\*\*This value is for analgesic effect.

### 2.1.4. Validation and calibration of the models

The validation of the models was done separately for all models. The skin model's validation for transdermal drug uptake is described elsewhere (Defraeye et al., 2020b, 2021).

**2.1.4.1 Validation of the PK model.** To validate the pharmacokinetics model, we used the experimental data of the concentration of fentanyl in the plasma over time from Marier et al. (2006). In this series of experiments, they analyzed 24 men aged 18–45 years, with a body mass of at least 60 kg and a body mass index of 18–26 kg/m<sup>2</sup>, which only 20 out of 24 men completed both periods of the trial. The participants were medically healthy, with clinically normal electrocardiograms (ECGs), and with no history of alcohol and drug abuse. The analysis was done over 11 days, with three fentanyl commercial patches with the nominal flux of 50 µg h<sup>-1</sup>, each for 72 hours. The PK parameters, which were used in this validation, are mentioned in Table 2, and the parameters for the mechanistic model, which indicates the incoming flux of fentanyl, are mentioned in Table 1.

**2.1.4.2. Calibration of the PD model for pain relief.** To develop a PD effect model for the VAS pain score, we used the reported VAS pain scores via the fentanyl plasma concentration of Sandler et al. (1992) work. In this study, 29 adult patients, aged between 18 and 80, and with weights less than 100 kg, under-treatment of intravenous fentanyl with an infusion rate of 1.0 µg kg<sup>-1</sup> h<sup>-1</sup> were analyzed. The model for the VAS pain score was assumed sigmoidal, which is mentioned in Equation 21. The baseline effect ( $E_{0, VAS}$ ), maximum effect ( $E_{max, VAS}$ , which here it is equal to  $E_{0, VAS}$ ), the concentration of the half-maximum effect ( $EC_{50, VAS}^{\gamma}$ ), and Hill coefficient ( $\gamma$ ) were obtained via fitting the model to experimental data and the resulting RMSD was 0.471.

## 2.2. Spatial and temporal discretization

The grid for the finite element method in each layer of the skin and patch was built based on the grid sensitivity analysis. In this sensitivity analysis, the spatial discretization error was considered 0.1% of the outgoing flux from the dermis layer, based on Richardson extrapolation. Therefore, the entire system's grid, including transdermal patch and skin layers, consisted of 110 quadrilateral finite elements. The

accumulation of grids is higher near the interface area to increase numerical accuracy. The duration of the simulations was 9 days (216 hours), which represents three periods of using fentanyl transdermal patch based on accepted therapy in the clinics. Based on the sensitivity analysis, the maximum time step should be 6 h. However, in this series of simulations, smaller time steps (0.1 h) were chosen to get a higher temporal resolution of the result.

## 2.3. Numerical implementation and simulation

COMSOL Multiphysics® software (version 5.5, COMSOL AB, Stockholm, Sweden), a finite-element-based commercialized software, was used in this study. The code developers verified this software. Therefore, the authors did not perform additional code verification. The mass transfer process of fentanyl through the patch and skin (drug uptake model) was carried out by the finite element method with a partial differential equations interface (coefficient form). Quadratic Lagrange elements were used with a fully coupled direct solver, which relied on the Multifrontal Massively Parallel sparse direct Solver (MUMPS) solver scheme. The drug distribution in the body, metabolism, and elimination (PK model) was modeled using the ordinary differential equations interface (in boundary domain). To track the changes in the concentration of fentanyl in the effect compartment (PD model), an ordinary differential equations interface was used. For evaluating the effect of fentanyl, based on the effect compartment fentanyl concentration at each time step, the boundary probe was implemented. The boundary probe was calculating the effect of the drug at each time step based on the current concentration of the drug in the effect compartment. The tolerances for solver settings and convergence were determined by means of sensitivity analysis in such a way that a further increase in the tolerance did not alter the resulting solution.

## 2.4. Computational configurations

### 2.4.1. Conventional fentanyl transdermal therapy

In clinics, the conventional therapy for fentanyl is to use a fentanyl patch for 72 hours and replace the patch, and the new patch needs to be placed on a new location body to avoid possible skin irritation (US Food and Drug

Administration, "Duragesic Label", 2005). To consider a period of therapy that includes the effect of changing patches in the process, we chose the duration of applying three patches (9 days). As the elimination path of fentanyl in the body is via the liver metabolism and renal elimination, the consumption of fentanyl for patients with severe hepatic or renal impairment should be monitored with caution. Additionally, as one of the important side effects of fentanyl is respiratory depression, patients with severe asthma or breathing problems should avoid fentanyl (US Food and Drug Administration, "Duragesic Label", 2005). In our model, as mentioned earlier, we changed the new patch's location; however, we assumed that the skin properties remain unchanged for different skin locations.

#### 2.4.2. Effect of age on the model parameters

The patient physiology affects drug uptake, distribution, metabolism, elimination, and its effects. Moreover, the impact of physiological features is different between different patients. Based on the studies, the patient's gender plays an important role in the outcome of fentanyl transdermal therapy. The gender of the patient will affect the stratum corneum, epidermis, and dermis thickness. Therefore, it affects the incoming amount of fentanyl to the body. Gender has an impact on pharmacokinetics model parameters and additionally on the activity of CYP enzymes. CYP enzymes are the main enzymes for fentanyl metabolism, which is the main elimination path for fentanyl. However, we only study the fentanyl transdermal therapy on one male patient; therefore, the gender of the patient is constant in this study. Based on the previous studies, the thickness of each layer of the skin changes by increasing age. The effect of age on each layer is not similar; for instance, as age increases, the thickness of SC will increase, while the thickness of the dermis will decrease (Robert and Robert, 2009; Boireau-Adamezyk et al., 2014). It should be noted that the changes in the dermis layer based on age were modified in this study to predict the changes in the equivalent thickness of the dermis based on age. Equation 14 (Boireau-Adamezyk et al., 2014) and 15 ((Modified) Robert and Robert, 2009) show the age's effect on each layer's thickness.

$$d_{sc}[\mu m] = 0.125 \text{ Age} + 11.800 \quad (14)$$

$$d_{Edm}[\mu m] = -2.25 \text{ Age} + 354.5 \quad (15)$$

The PK parameters do not show significant changes based on age (Scott and Stanski, 1987); therefore, in this study, we assume the PK parameters are the same for the virtual patient of different ages. Despite PK parameters, Scott and Stanski (1987) showed that the required opioid dose for reducing the intensity of electroencephalography (EEG) reduces by increasing age. They studied the effect of fentanyl on 20 patients with age between 20 and 88 years. They were all male and without any renal or hepatic disease. They found a relationship between age and concentration of the half-maximum effect of fentanyl for the effect of the reduction of EEG. In this study, we assumed the normalized rate of changes in  $EC_{50}$  for the reduction of EEG by age is similar to the reduction of VAS pain score. The derived equation for

changes in half-maximal effective concentration for VAS pain score, which is modified from EEG result to be used for VAS pain intensity, is mentioned in Equation 16.

$$EC_{50}^{VAS} [ng \text{ ml}^{-1}] = -1.148 \times 10^{-2} \text{ Age} + 1.96 \quad (16)$$

By aging the response of a patient to fentanyl transdermal therapy based on the effect on ventilation rate might changes as well. Including this change in the model helps to better control the therapy; however, due to lack of sufficient data, we did not consider it.

#### 2.4.3. Individualized therapy with a precalibrated digital twin

In the first step, we did not consider the virtual patient feedback in the model, which we refer to this twin as a precalibrated digital twin. The twin is customized to the patient class by calibrating it in advance for a certain age class, using Equations 14–16. By using this precalibrated digital twin, the VAS pain score of the virtual patient was calculated at each time. Based on the pain level of the virtual patient, the decision of keeping the patch on or changing it will be made. In this process, the type of fentanyl patch has not been changed, and it has the properties of a Duragesic® fentanyl patch with a nominal flux of  $75 \mu\text{g h}^{-1}$ . The considered criteria for changing the patch are that the VAS pain score is above 3, while the gradient of pain is positive (pain is increasing). A VAS pain score at or under 3 means the pain level is in the mild range; therefore, we considered the VAS pain score 3 as the target treatment to check for changing the patch. When the VAS pain score goes under 3, the patch will remain on the skin until the VAS pain score goes above 3, again. The strategy of changing the patch based on the pain is represented in a flowchart in Figure 3a.

#### 2.4.4. Personalized therapy real-time digital twin

Due to the complex nature of the human body and the changes that happen to patient response, the calculated VAS pain score might have a deviation from the real VAS pain score. To take this effect into account, we mimicked a different patient response for 100 patients. With a real-time digital twin, the patient's VAS pain score will be taken from the virtual patient at defined time intervals, and the calculation will be updated with these data. To include the virtual patient's real VAS pain score in the model, we assumed that the virtual patient would enter the VAS pain score (integer numbers between 0 and 10) every 24 hours to the model. Another assumption for patient feedback was that the maximum difference between patient pain intensity and calculated pain is two VAS units. We produced a set of random feedback by considering the mentioned assumptions (deviation from calculated pain by PD model) via MATLAB®. The produces random deviation from calculated pain is shown in Figure 4. The flowchart of the strategy of updating the digital twin based on the virtual patient VAS pains score data is shown in a flowchart in Figure 3b.



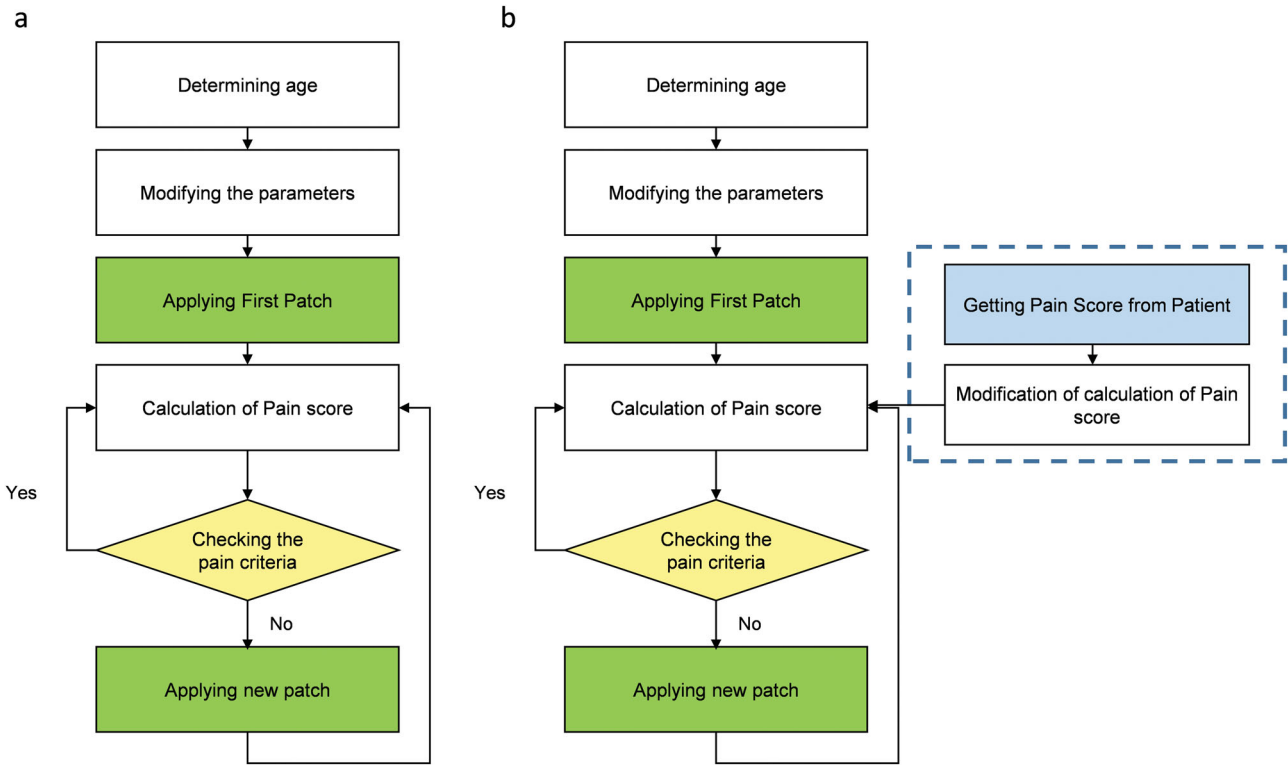


**Figure 3.** (a) Flowchart of making the decision for changing the patch based on the VAS pain score calculation. (b) Flowchart of making the decision for changing patch based on VAS pain calculation updated by virtual patient feedback.

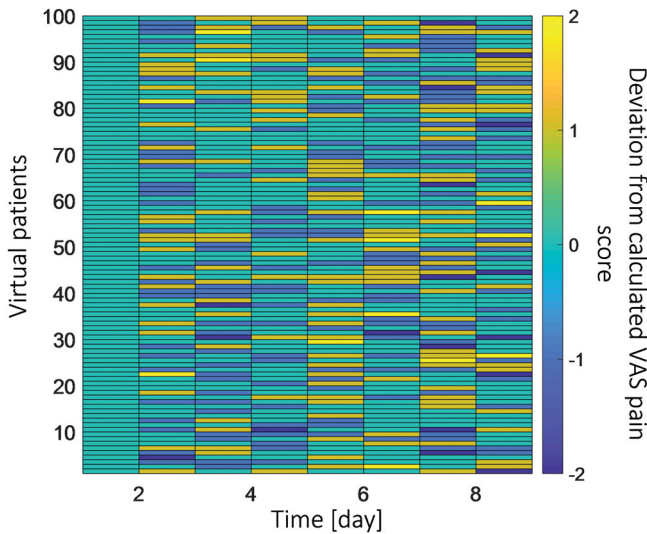


**Figure 4.** The set of random deviations from the calculated VAS pain score for 100 virtual patients at 8 feedback moments for 9 days.

**2.5. Metrics**

The process of drug delivery from the patch to the site of action was analyzed by several metrics. These metrics are the remaining drug in the patch ( $m_{pt}$ ), total delivered drug to the skin ( $m_{ts}$ ), and amount of drug in the skin ( $m_s$ ) as a function of time. Another important metric in this study is time without pain, which was considered the time that the VAS

pain score is under 3 during the treatment period. The remaining drug content ( $m_{pt}(t)$ ) in the patch is being calculated as a function of time, which is being reduced based on outgoing flux from the patch. The calculation for  $m_{pt}(t)$  is brought in Equation 17.

$$m_{pt}(t) = m_{pt}^0 - \int_0^t drug\ flux\ out\ of\ patch .dt \quad (17)$$

where  $m_{pt}^0$  is the initial amount of drug in the patch. The total delivered drug ( $m_{ts}(t)$ ) to the body can be calculated based on the patch’s remaining drug. Equation 18 demonstrates the calculation of the total delivered drug to the body.

$$m_{ts}(t) = \sum_{i=1}^n (m_{pt, i}^0 - m_{pt, i}(t)) \quad (18)$$

where  $n$  is the number of patches that are used during a certain period of therapy. The amount of drugs in the skin is related to the incoming flux of drugs from the patch and outgoing flux to the blood circulation. This variable can be calculated based on the concentration of drugs in skin layers which is calculated by Fick’s second law. The calculation of the amount of drug in the skin ( $m_s(t)$ ) is shown in Equation 19.

$$m_s(t) = \int c(t, x).dV_s \quad (19)$$

where  $V_s$  is the volume of the skin. Regarding the time without pain, as previously mentioned, we sum up the times that the VAS pain score is under 3.

## 2.6. Sensitivity analysis of the model parameters

The sensitivity of the total delivered drug from the skin ( $m_{ts}$ ), average fentanyl plasma concentration during 72 hours ( $\overline{c_{p,72}}$ ), and the average VAS pain score to the related parameters were studied. These parameters are related to drug uptake (partition coefficient, diffusion coefficient, layer's thickness), PK (compartment's volume, blood flow between compartments, clearance coefficient, and the fraction of unbound drug), and PD (half-maximal effective concentration and Hill coefficient) model. The sensitivity index in this study was calculated for each parameter based on Equation 20.

$$SI = \frac{U_{x_{i+1}} - U_{x_{i-1}}}{\Delta x_i} \frac{x_i}{U_{x_i}} \quad (20)$$

where  $x_i$  is the model input parameter and  $U_{x_i}$  is the dependent variable ( $m_{ts}$ ,  $\overline{c_{p,72}}$ , or VAS pain score) corresponded to  $x_i$ . SI is the sensitivity index, which we use to analyze the sensitivity of  $U_{x_i}$  to  $x_i$ . Here, we considered  $\frac{\Delta x_i}{x_i}$  as 1%, to evaluate the sensitivity index based on this 1% deviation from the chosen value for  $x_i$ . The result of sensitivity analysis is shown in [supplementary materials](#).

## 3. Results and discussion

### 3.1. Validation of the PK model

To evaluate the validation of results from the pharmacokinetic model, we compared our result with Marier et al. (2006), in which the detail of the experiment is provided in section Validation of the PK model. The results of the simulation and the average results of the experiments (Marier et al., 2006) are shown in Figure 5. The root-mean-square deviation (RMSD) of simulation data and experimental data was 0.152 [ng ml<sup>-1</sup>]. By analyzing the result from simulation and the experiment, we find at the beginning there is a time difference for reaching the maximum concentration for the first peak; however, this difference is less for the next two peaks. In the experiment, in the third peak, there is a jump in the concentration, which the simulation could not predict. This jump could be due to changes in the situation for patients or the measuring process of the concentration of

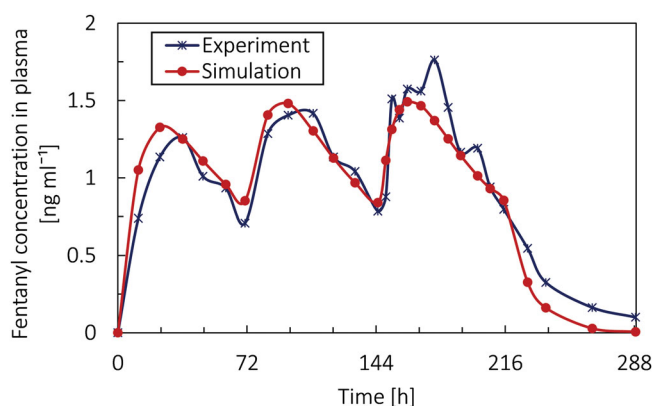


**Figure 5.** The concentration of fentanyl in the blood circulation system ( $c_p$ ) as a function of time from experiment and digital twin over 11 days by applying 3 patches with the nominal flux of 50  $\mu\text{g h}^{-1}$ , each for 72 hours following two days with no patches.

fentanyl in plasma. However, in general, the agreement of the model with the experiments is satisfactory. However, in the following part of this study, the Duragesic fentanyl patch with a nominal flux of 75  $\mu\text{g/h}$  is being used to reach the pain intensity target.

### 3.2. Calibrating the PD model for VAS pain score

As mentioned in section 2.1.4.2, we obtained the value of constants for sigmoid function related to the relationship between VAS pain score and fentanyl concentration in the effect compartment (Equation 22) based on experimental data. In Figure 6, the average experimental VAS pain score (Sandler et al., 1992) and simulated PD model data are shown. The corresponding simulated plasma fentanyl concentration is demonstrated in the subplot. Based on the fitted sigmoidal model, as concentration increases, the pain intensity decreases. For instance, from  $t=4$  h to 8 h the patient's pain intensity has a plateau while the concentration of fentanyl is increasing in the blood and subsequently in the central nervous system. This different behavior could be due to several reasons, such as the time lag between drug concentration and effect, deviance from measure concentration, and the overall average concentration of drug in plasma. However, in general, the agreement of the model with the experiments is satisfactory, and the percentage error is within 8.9%.

$$E_{VAS} = E_{0, VAS} - E_{max, VAS} \times \frac{c_{e, VAS}^{\gamma}}{EC_{50, VAS}^{\gamma} + c_{e, VAS}^{\gamma}} \quad (22)$$

### 3.3. Analysis of conventional fentanyl transdermal therapy

At first, the drug uptake, PK, and PD simulations were performed for conventional transdermal therapy for a virtual patient at age 20 years. In Figure 5, the fentanyl flux released from the patch and out of the dermis is shown. When a patch has been placed, there is a peak in the drug flux out of the patch. The maximal flux out of the patch for the first patch was 398  $\mu\text{g cm}^{-2} \text{h}^{-1}$ , which occurred in one hour of

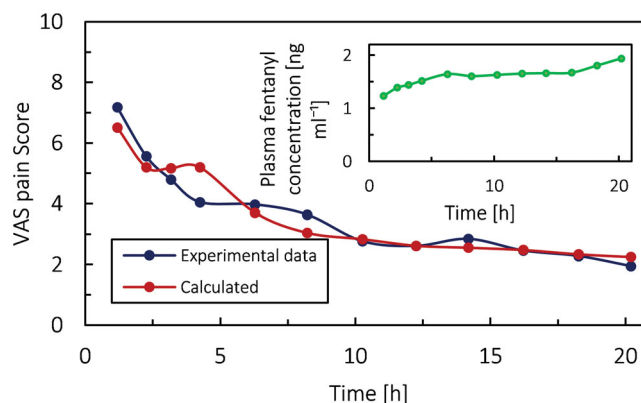


**Figure 6.** Average experimental VAS pain score during fentanyl therapy and fitted data. Subplot: concentration of fentanyl in the blood circulation system, for infusion rate of 1.0  $\mu\text{g kg}^{-1} \text{h}^{-1}$ .

applying the patch. After applying the patch, the outgoing flux of fentanyl from the patch decreases drastically; in a way, the outgoing flux of fentanyl reaches  $6.85 \mu\text{g cm}^{-2} \text{h}^{-1}$  after 1 h and  $0.95 \mu\text{g cm}^{-2} \text{h}^{-1}$  after 72 h. After releasing the drug from patch to skin, due to the low diffusion coefficient and thickness of skin, there is a time lag to reach the maximum flux of outgoing drug from the skin. As the drug gradually leaves the dermis, the outgoing drug flux from the skin does not change drastically, unlike the patch. As shown in Figure 7, the maximal flux out of the dermis was  $2.31 \mu\text{g cm}^{-2} \text{h}^{-1}$ , and it occurred after 19 hours after applying the patch, and the average flux out of the dermis during 72 hours is  $1.47 \mu\text{g cm}^{-2} \text{h}^{-1}$ . The delay in drug uptake between the dermis and patch is clear and spans several hours. This shows the slow response and thus the need for proper control of transdermal therapy.

The initial amount of fentanyl in the patch was 12.6 mg/mg for the Duragesic® fentanyl patch with a target nominal flux of  $75 \mu\text{g h}^{-1}$  (with  $30 \text{cm}^2$  surface area). After applying the patch, the drug diffuses from patch to skin and is eventually uptaken by the blood circulation system in the dermis. Figure 6a shows that after 72 hours, the amount of fentanyl in the patch reduces from 12.6 mg to 8.99 mg, which means during 72 hours, only 28.6% of the drug in the patch

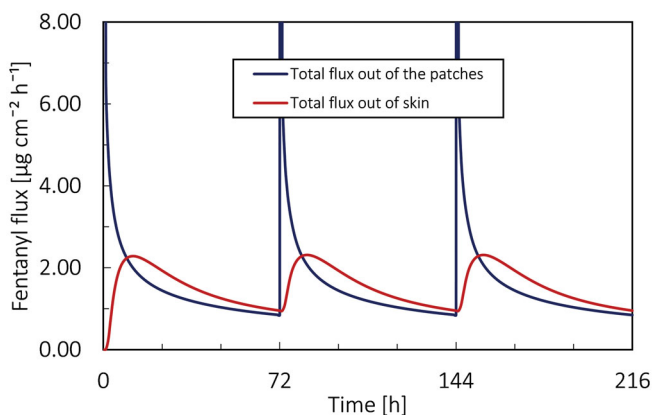


**Figure 7.** Fentanyl flux at skin-patch and dermis-blood circulation interface during 9 days by applying 3 patches of fentanyl with the nominal flux of  $75 \mu\text{g h}^{-1}$  each for 72 hours.

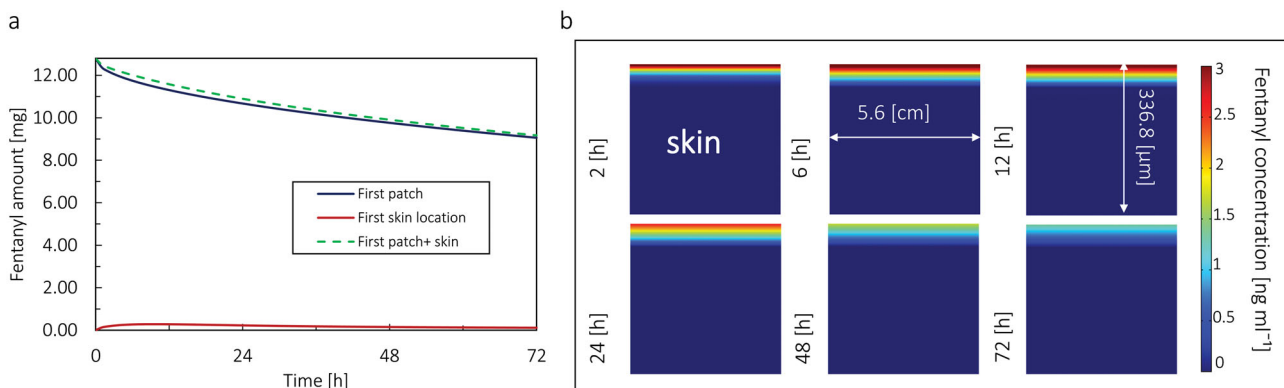


**Figure 8.** (a) Amount of fentanyl stored in the patch, skin, and cumulative amount fentanyl in skin and patch in 72 h by applying one patch. (b) The concentration of fentanyl in skin layers in 72 h for the virtual patient at the age of 20 years.

was used. Simultaneously, the amount of fentanyl in the skin after 15 hours increased from 0 mg to reach its maximum at 0.843 mg, and then it decreased to 0.528 mg at the end of 72 hours. The difference between the total drug in the skin and patch together from the patch's initial drug content is the amount of drug taken up from the skin by blood circulation. Figure 6b shows that the fentanyl concentration in skin layers is shown, which shows that the fentanyl is more accumulated in the upper part of the skin close to the patch, as expected (Figure 8).

From the PK simulation, the concentration of fentanyl in each compartment for the virtual patient at the age of 20 years is shown in Figure 9a. The concentration profile of fentanyl is based on the parameters mentioned in Table 2. The maximum plasma concentration for fentanyl after applying the first patch is  $1.86 \text{ng ml}^{-1}$ , which occurs 22 h after applying the first patch. Based on the literature, for the Duragesic® fentanyl patch with a surface area of  $30 \text{cm}^2$ ; the nominal flux is  $75 \mu\text{g h}^{-1}$  (Nelson and Schwaner, 2009); however, based on our result, the fentanyl flux from the patch is highly time-dependent and far from being constant. The mean  $C_{max}$  of fentanyl is reported  $1.7$  (SD = 0.7)  $\text{ng ml}^{-1}$  and the average time to reach the maximum concentration of drug in plasma is 33.5 h (SD = 14.5) (Nelson and Schwaner, 2009). The difference between the obtained results from our simulation and reported averages is less than one standard deviation. The maximum fentanyl concentration in slow equilibrated, rapid equilibrated, gastrointestinal, and hepatic compartments is 13.96, 0.27, 0.31, and  $0.08 \text{ng ml}^{-1}$ , respectively. Time for maximum concentration ( $t_{max}$ ) for the slow equilibrated compartment is 31 [h], and for the other compartments is 23 h. By comparison the concentration profile of fentanyl in slow equilibrated and central compartment, we realize due to the lipophilicity of fentanyl, most of the drug is accumulated in adipose tissue. In Figure 9b, the plasma fentanyl concentration (fentanyl concentration in the central compartment) for one transdermal patch over 216 h is shown. Based on the literature, the minimum therapeutic level for fentanyl is  $0.63 \text{ng ml}^{-1}$ , while the minimum toxic concentration is  $2 \text{ng ml}^{-1}$  (Jeal and Benfield, 1997, Schulz and Schmoldt, 2003). For our base case, after 7.62 h, the fentanyl concentration in the virtual patient

reached the therapeutic range (0.63–2 ng ml<sup>-1</sup>) and remained in this range for the following 208 hours. It should be mentioned that the therapeutic range is different for each person, and the shown therapeutic range is just an average.

In Figure 10, the fentanyl concentration in plasma is shown for the effect compartment of ventilation and

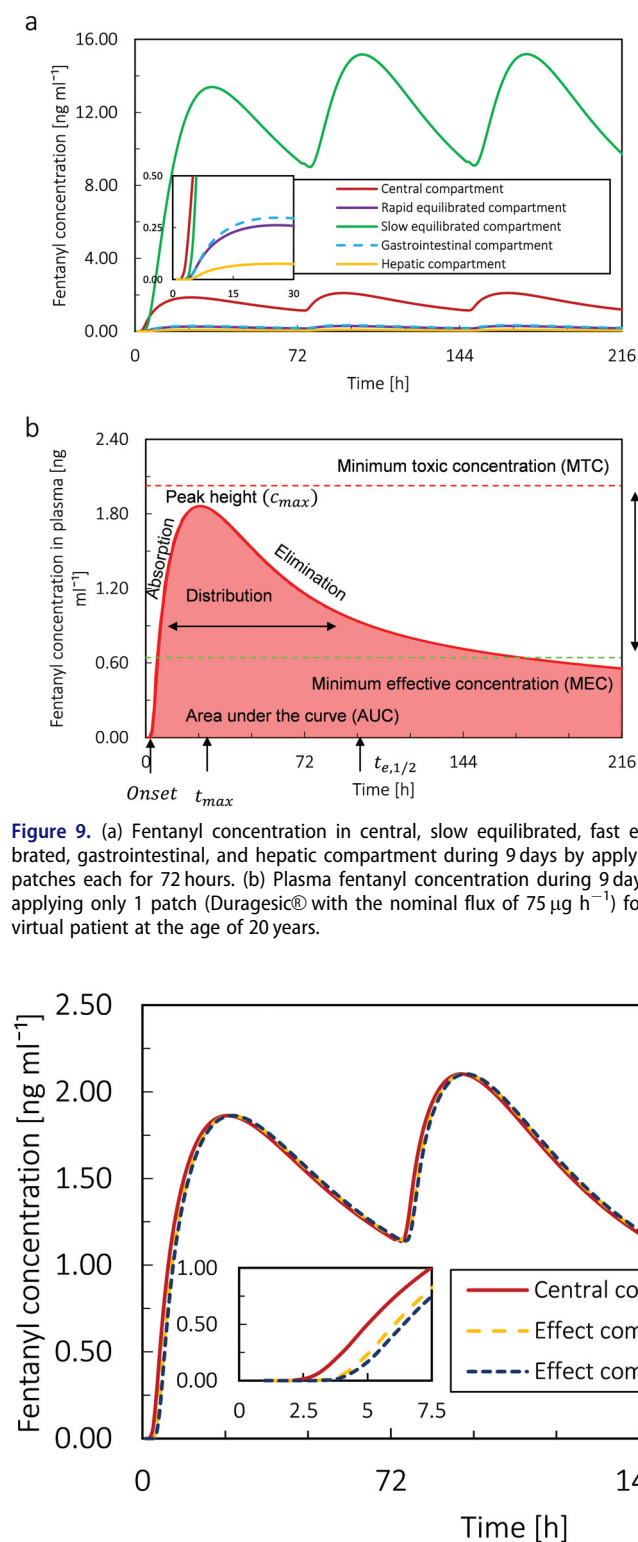


**Figure 9.** (a) Fentanyl concentration in central, slow equilibrated, fast equilibrated, gastrointestinal, and hepatic compartment during 9 days by applying 3 patches each for 72 hours. (b) Plasma fentanyl concentration during 9 days for applying only 1 patch (Duragesic® with the nominal flux of 75 μg h<sup>-1</sup>) for the virtual patient at the age of 20 years.

analgesia. The calculation of concentration in effect compartment-based plasma concentration is described in Equation 12 in section Mechanism-based pharmacodynamics model. The effect compartment only produces a delay between the concentration of fentanyl in plasma and the effect of the drug. As the result shows, the concentration profiles are very close to each other. This is due to the high potency of fentanyl, which facilitates the passage through the blood-brain barrier (BBB) (Chaves et al., 2017). This minor difference between these three concentration profiles is due to the different first-order equilibrium rate constant for each effect compartment.

Pain relief and reduction of ventilation rate for the patient after applying fentanyl patch are related to the concentration of fentanyl in the plasma. Based on the conventional therapy results for the virtual patient at the age of 20 years, as the plasma fentanyl concentration increased, the ventilation rate and VAS pain score dropped. When the fentanyl concentration in the plasma reaches its maximum, the rate of change in the plasma concentration decreases. The reduction in plasma concentration gradient also changes the gradient in

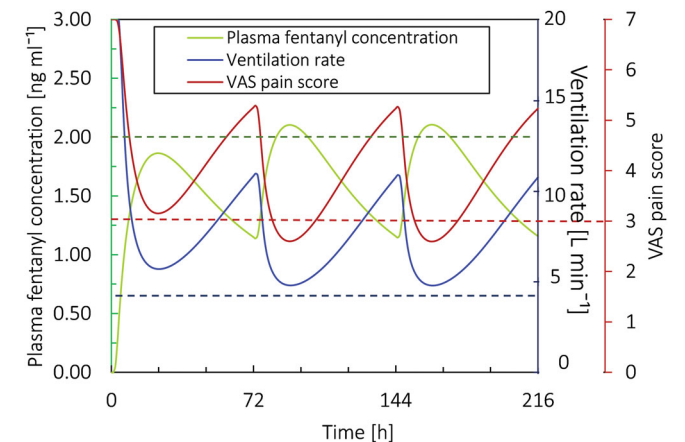


**Figure 11.** Ventilation rate, VAS pain score, and plasma fentanyl concentration for the base case for 9 days by applying 3 patches each for 72 hours.

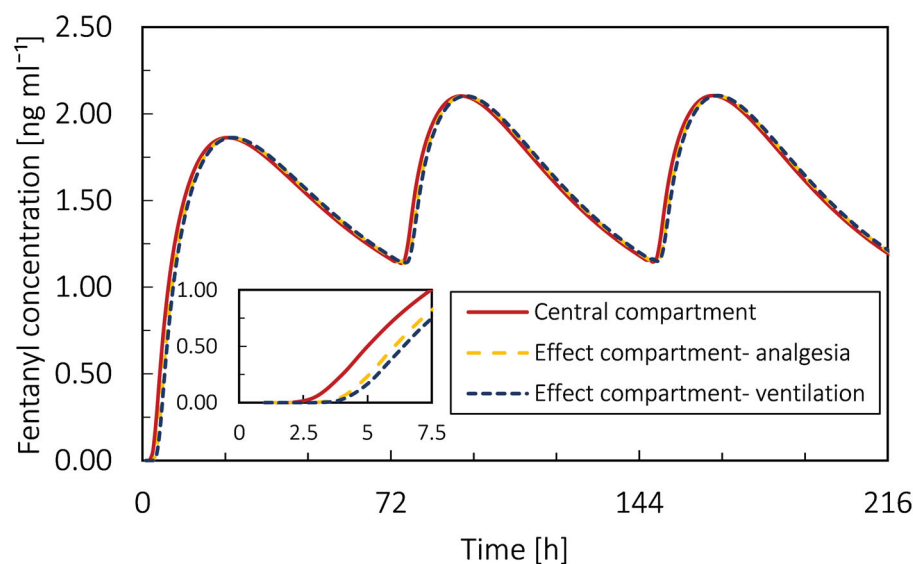


**Figure 10.** Fentanyl concentration in the central compartment, effect compartment for ventilation, and effect compartment for analgesia for 9 days by applying 3 patches each for 72 hours.



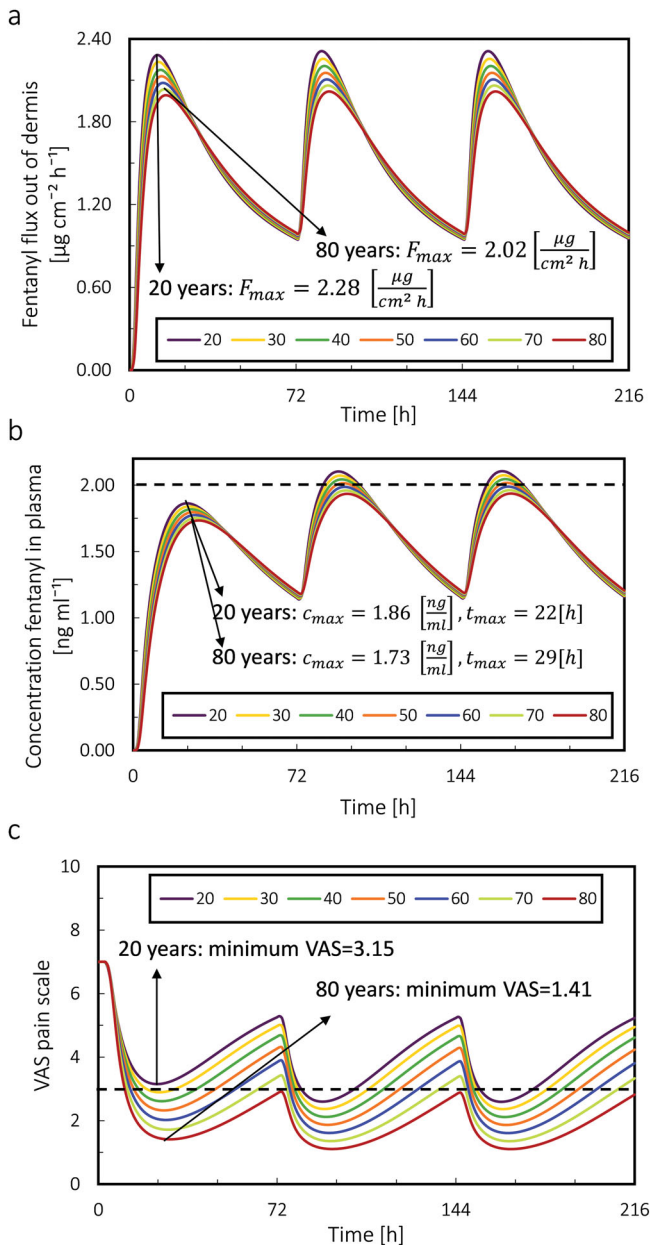


**Figure 12.** (a) Fentanyl flux out of dermis; (b) Plasma fentanyl concentration. The dotted line is the concentration threshold in plasma; (c) VAS pain score for the virtual patient with different ages from 20 years old to 80 years old during 9 days by applying 3 patches each for 72 hours. The dotted line is the pain intensity target.

pain intensity and reduction of ventilation rate. Therefore, after reaching the  $c_{\text{max}}$  of the first patch, the fluctuation in pain intensity and ventilation rate reduces. It should be noted that the threshold for fentanyl concentration in plasma which is shown in Figure 11, is an average number for the patients. On the other hand, in this study, we only considered the reduction in minute ventilation as the adverse effect; however, fentanyl therapy can cause other adverse effects such as nausea.

### 3.4. Effect of age on the therapy

The stratum corneum is the main obstacle in the drug penetration path through the skin into the blood circulation

system. As age increases, the thickness of the SC increases, and the thickness of the dermis decreases. Therefore, the increase in SC thickness will reduce the amount of fentanyl delivered to the body and lead to a delay and reduction of drug uptake. As shown in Figure 12a, the effect of increasing thickness of the SC on drug flux out of the skin is more than the effect of decreasing thickness of the dermis. Based on this result, as age increased, the maximum flux decreased, and the time to reach this maximum flux increased. From age 20 to 80 years, the maximum flux of drugs into the blood decreased by 11%, and the time to reach this maximum flux increased by 15%. This implies that by applying the same fentanyl patch for the patient at different ages, the patient uptakes less amount of fentanyl by aging. Simultaneously, the time to reach the maximum flux of the drug increases.

In this study, we assumed that the PK parameters do not change with age. However, as the age changes, the drug flux out of the dermis will change. Consequently, the different blood drug uptake, which is a result of different drug flux out of the dermis, changes the concentration of drugs in PK compartments. Figure 12b shows that the maximum concentration of fentanyl from age 20 to 80 years decreases by 7%, and the time to reach this maximum increased by 32%. The reduction of  $c_{\text{max}}$  and the increase in  $t_{\text{max}}$  by increasing age are also reported in other works such as Thompson et al. (1998) and Paut et al. (2000). The result implies that even if the patient at different ages receives the same therapy, by aging, the accessible drug amount for the patient for pain relief (concentration of drug in plasma) reduces.

Based on the result of drug uptake and PK modeling, the virtual patient at older ages received less amount of drug, which led to lower fentanyl plasma concentration. As mentioned in the material and method section (section Effect of age on the model parameters), the fentanyl concentration required to reach the half-maximum effect will be reduced by aging. The result of PD, shown in Figure 12c, shows that, despite receiving less fentanyl, the VAS pain score in older age was reduced more than in younger age. The reduction in VAS pain score for the patient at the age of 80 years was 55% more than the age of 20 years. The reduction of required opioids for pain relief with increasing age is reported in other works too (Scott and Stanski, 1987; Rees, 1990; Macintyre and Jarvis, 1996; Woodhouse and Mather, 1997). To summarize the result of this section, if a similar fentanyl therapy is being applied for the patient, by increasing the age, the patient receives less amount of drug. However, the patient might still experience more pain relief as opioid requirements for pain relief decrease by age.

### 3.5. Individualized therapy with a precalibrated digital twin

As mentioned in the previous section, virtual patients of different ages received different amounts of the drug and showed different levels of pain relief. Therefore, it is actually needed for each virtual patient in a certain age category to receive a different therapy to reach desirable pain relief.

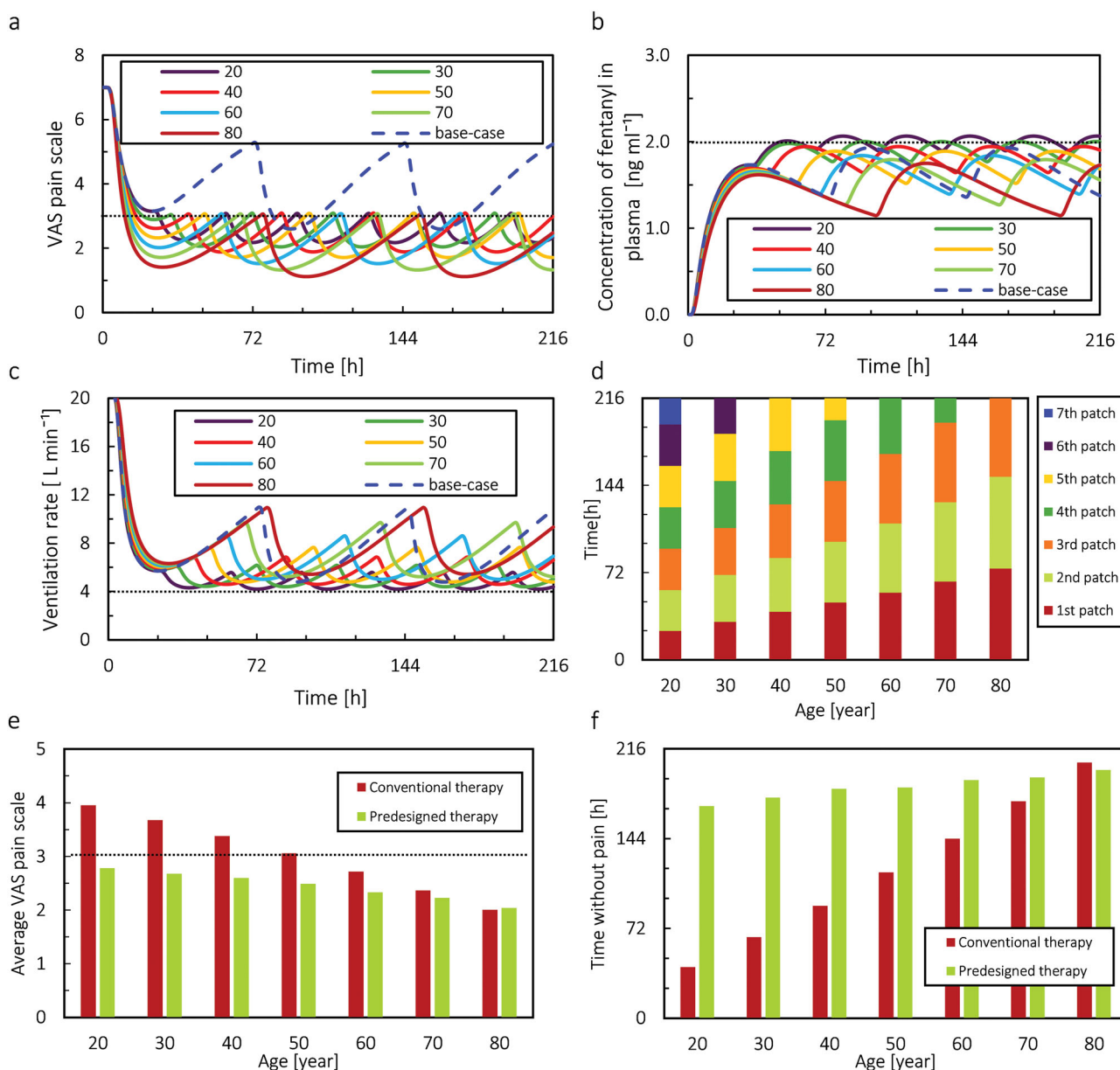


**Figure 13.** (a) VAS pain score versus time for predesigned therapy. The dotted line represents the target pain intensity. The base case is conventional therapy for 20 years old virtual patients. (b) Fentanyl plasma concentration versus time for predesigned therapy. The dotted line represents the threshold for fentanyl concentration in plasma. The base case is conventional therapy for 20 years old virtual patients. (c) The ventilation rate versus time for predesigned therapy. The base case is conventional therapy for 20 years old virtual patients. The dotted line represents the minimum normal ventilation rate. (d) Duration of applying each patch. (e) The average VAS pain scores both for conventional therapy and for proposed pain control therapy. The dotted line represents the target pain intensity. (f) The time that patient VAS pain score was under 3, which we assumed as time without pain for virtual patients with 20–80 years old during 9 days both for conventional therapy and proposed pain control therapy.

Using a precalibrated digital twin of the patient in a certain age category, we composed a more suitable therapy for each age category. The fentanyl concentration and VAS pain score for different age categories are shown in Figure 13a,b. The results in these two graphs show that the precalibrated therapy by digital-twin successfully kept the pain intensity below the target by slightly increasing in concentration of fentanyl in plasma and keeping it in almost constant value. This increase in concentration was only done by changing the frequency of replacing the patch. Another criterion in the proposed therapy by digital twin was avoiding respiratory depression, which we monitored by ventilation rate. Results in Figure 13c show, despite the increase in the

concentration of fentanyl in plasma, the digital-twin suggested therapy tried to keep this increasing at a minimum level to avoid hypoventilation.

As shown in Figure 13d, virtual patient of different ages needs a different number of patches in the same time frame, with different durations of application. In conventional 3-day therapy for 216 hours, only 3 patches will be applied. However, for achieving a therapy where the pain score shall be kept under 3 for the age of 20 years, almost 7 patches are needed. Based on these results, by aging, the patient needs to change the patch less frequently. The result in Figure 13e shows that by applying the proposed age-dependent therapy, the average pain intensity for the patient at the age of

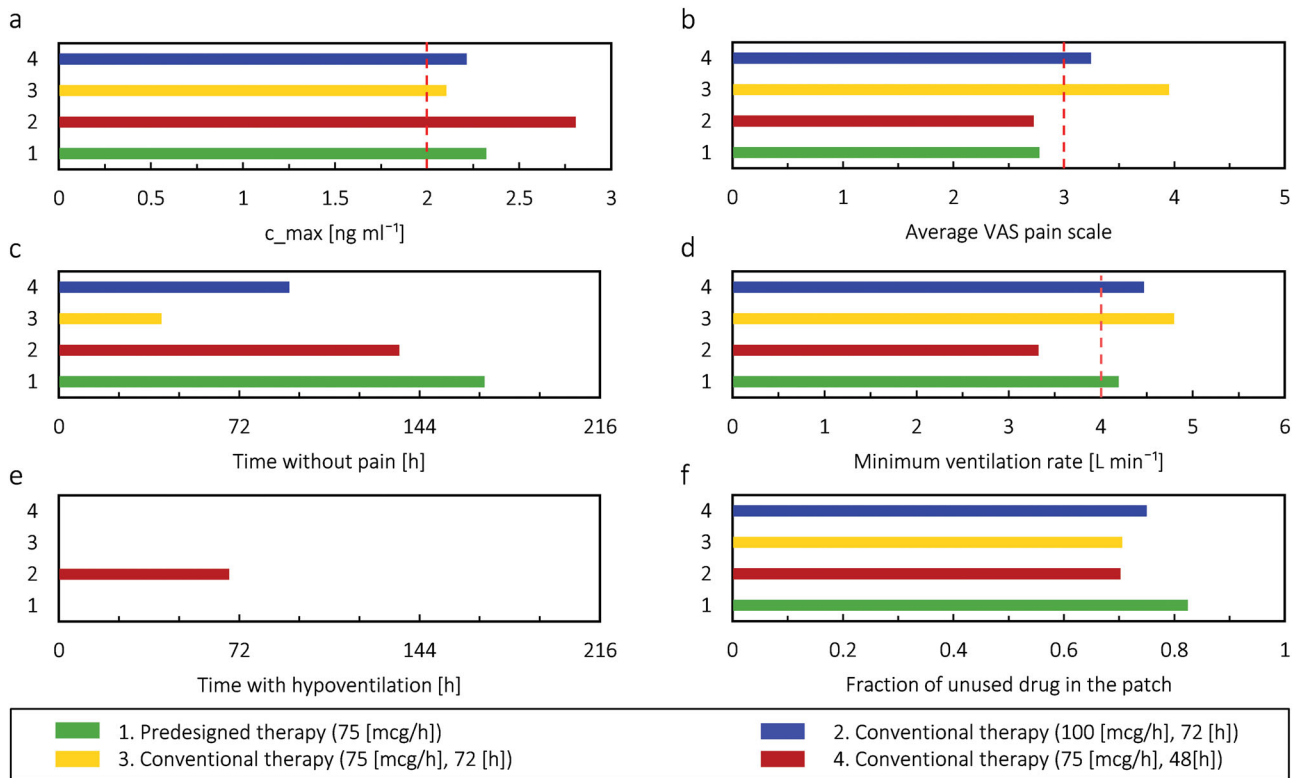


**Figure 14.** comparison of four therapies (predesigned therapy with digital twin and three conventional alternative therapies). (a) maximum concentration of fentanyl; (b) average VAS pains score, (c) time without pain; (d) minimum ventilation rate, (e) duration of hypoventilation; (f) the fraction of unused drug in patch during 9 days for the virtual patient at the age of 20 years.

20 years decreased by 30%. Therefore, the change in time of replacing the patch led to better performance of proposed therapy by digital twin compared to conventional therapy in relieving the pain. Note that we could also adjust and change therapy by using patches with different concentrations as well, but this we did not explore.

As mentioned in previous paragraphs, the aim of the proposed therapy by digital twin was to keep the VAS pain score under 3 while keeping the plasma concentration at the lowest possible amount to reach this target. Here we calculated the duration of which the pain intensity was below 3, which we call time without pain, as a parameter to evaluate the success of the treatment. The result in 3/f shows that the digital twin increased the time without pain considerably. For the virtual patient at the age of 20 years, the time without pain increased by 314%. As mentioned in section Individualized therapy with a precalibrated digital twin, decreasing pain intensity to a much lower value than 3 is not the aim of this study; however, it is important to keep it under 3 while avoiding therapy's adverse effects. By implementing the digital twin, we were successful in keeping the VAS pain score under 3 for a longer period of time. Therefore, considering the presented result in Figure 13, the digital twin successfully decreased the pain intensity and increased the time without pain. Meanwhile, the increase in the concentration of drug in plasma was at a controllable level, in which the virtual patient did not face hypoventilation in the period of the therapy. The fluctuations in drug concentration, VAS pain score, and ventilation rate were the smallest for young patients as they needed to replace the patch more frequently.

The predesigned therapy by a precalibrated digital twin proposed that 3 patches with the nominal flux of  $75 \mu\text{g h}^{-1}$  for 9 days are not sufficient in order to reach the favorable pain relief for the patient at the age of 20 years. However, it would suffice for an 80-year-old patient. This therapy suggested the patch needs to be changed more frequently to keep the VAS pain score under 3. In the clinics, when the applied fentanyl patch is not efficient for pain relief, there are two other options. First, change the patch at each 48 h instead of 72 h (US Food and Drug Administration, "Duragesic Label", 2005); second, change the patch to a higher dose. Here we compared the performance of four different therapies for the virtual patient at the age of 20 years: 1. Predesigned therapy by digital twin with fentanyl patch with the nominal flux of  $75 \mu\text{g h}^{-1}$ ; 2. Using fentanyl patch with the nominal flux of  $100 \mu\text{g h}^{-1}$  and changing at each 72 h so conventional therapy at a higher dose; 3. Using fentanyl patch with the nominal flux of  $75 \mu\text{g h}^{-1}$  and changing at each 72 h so conventional therapy; 4. Using fentanyl patch with the nominal flux of  $75 \mu\text{g h}^{-1}$  and changing at each 48 h. It should be noted the last three therapies in the list are conventional therapies that are used in the clinics.

The result of this comparison is shown in Figure 14. The maximum concentrations of fentanyl in plasma for all these four approaches are above the  $2 \text{ ng ml}^{-1}$  threshold, but it was necessary to reach the target pain relief (Figure 14a). The result shows by digital twin therapy, the VAS pain score is at the favorable level (under 3) and time without pain has the highest value compared to the other three approaches (Figure 14b,c). The second approach (using fentanyl patch

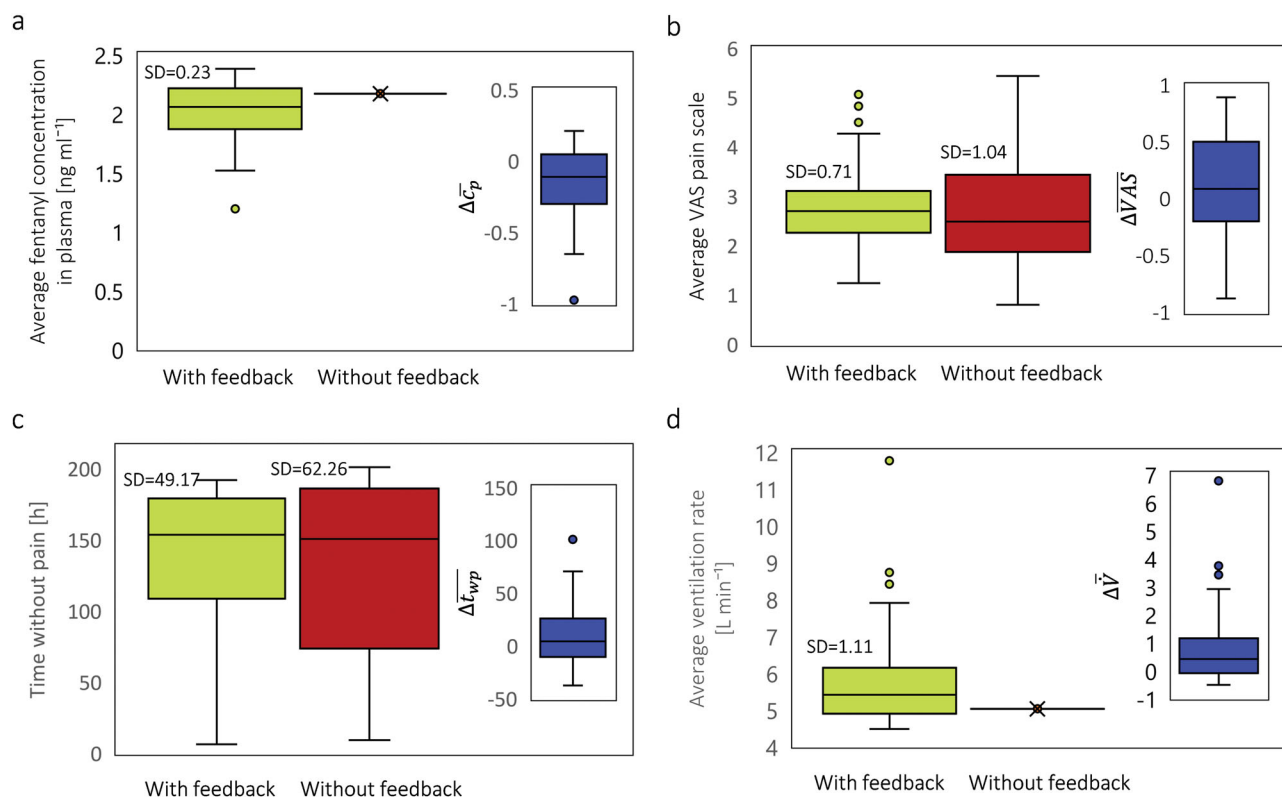


**Figure 15.** (a) Distribution of average plasma concentration of fentanyl; (b) Distribution of average VAS pain score; (c) Distribution of time without pain; (d) Distribution of average ventilation rate for the same population of 100 virtual 20 years old patients for 9 days both for pain control therapy by including feedback and without including feedback. The results are for the same virtual population with 100 members.

with the nominal flux of  $100\ \mu\text{g h}^{-1}$  was not successful in keeping the ventilation rate in the normal range (Figure 14d,e), while the other three approaches managed to do it. However, it was successful in keeping the VAS pain score below 3. As in predesigned therapy by digital twin, the change of the patch (with the nominal flux of  $75\ \mu\text{g h}^{-1}$ ) was more frequently; the fraction of unused drug in the patch for this approach compared to the other three approaches is higher by 17.1%, 17%, and 9.3% respectively (Figure 14f). To summarize this comparison, using the patch with the nominal flux of  $75\ \mu\text{g h}^{-1}$  and changing every 72 h (third approach) or using the patch with the nominal flux of  $75\ \mu\text{g h}^{-1}$  and changing every 48 h (fourth approach) is not very effective in pain relief. Therefore, based on the main criteria for pain management, the best solution can be chosen. For the aim of keeping the pain under VAS pain score 3, the first and second approaches can meet the requirements. On the other hand, the second approach was not able to avoid hypoventilation. When we want to achieve sufficient pain relief ( $\text{VAS} < 3$ ) and a sufficiently high ventilation rate, only predesigned therapy by digital twin meets all the criteria; however, it should be noted the frequency of changing the patch affects the cost of the therapy as more patches are needed.

### 3.6. Individualized therapy by the real-time digital twin

To evaluate the effect of patient feedback in the digital twin's proposed therapy, we assumed 100 virtual patients with the same physiological state as the 20 years virtual

patient. This means all these 100 virtual patients had the same model input parameters but varied in their feedback response to the treatment. These virtual patients fed their VAS pain score into the model based on the procedure mentioned in the section Personalized therapy real-time digital twin. In this approach, sometimes, the patient will thereby not receive the required amount of fentanyl, and sometimes, the patient receives an extra amount of drug, which is not necessary. As a result of including patient feedback, the pattern of replacing the patch was changed in order to meet the patient's needs. To compare the performance of this feedback approach with the one in section Analysis of conventional fentanyl transdermal therapy, we evaluated the average fentanyl plasma concentration, VAS pain score, time without pain, and ventilation rate.

In Figure 15a, the result shows that in most cases, the average fentanyl concentration was lower compared to the therapy proposed by the precalibrated digital twin. If we apply a *t*-test on the result of these two therapies, the obtained *p*-value is  $1.8 \times 10^{-8}$ , which implies the difference in the plasma concentration for both approaches is significant. The blue boxplot at each graph represents the difference between the corresponding values between two approaches for every single patient. In Figure 15b, the average VAS pain score via the two approaches is shown. Based on the result, the median of average VAS pain score is higher for the therapy with the feedback. However, the *p*-value for pain intensity between these two approaches is 0.32, which implies there is no significant difference in the average VAS pain score via these two approaches. Therefore, we can



conclude including patient feedback does not have a significant effect on the pain relief performance of the digital twin.

In [Figure 15c](#), the time without pain for each case via two approaches is shown. The results show that the median time without pain is higher by 3 hours for the digital twin with patient feedback. Additionally, the standard deviation for the digital twin with the patient feedback approach is lower than without the patient feedback approach by 10%. However, the  $p$ -value of the difference between times without pain via these two approaches is 0.25, which implies no significant difference between them. In the digital twin with patient feedback approach, when the patch is changed is based on the updated VAS pain score, the fentanyl plasma concentration varies individually. Therefore, the ventilation rate will be different for all these 100 cases. In the digital twin without patient feedback approach, as the patches will change at the same time for all these 100 cases, the plasma fentanyl concentration will be the same for all of them; therefore, the average ventilation rate was  $3.9 \text{ L min}^{-1}$  for all the cases. The result in [Figure 15d](#) demonstrates that by considering feedback, more than 50% of the patients have a higher ventilation rate than the approach that we did not consider the patient's feedback. This is the result of not delivering an extra amount of drug to the patient. For the patients with a lower ventilation rate, the patient needed more amount of fentanyl to reduce the pain level. Therefore, the ventilation rate was lowered. The decision-making criteria to change the patch in this study were done only based on the VAS pain score, not a combination of VAS pain score and ventilation rate. The result of the  $t$ -test for ventilation rate via these two approaches is  $5.9 \times 10^{-8}$ , which refers to a significant difference between these two approaches. We can conclude that the reduction in plasma concentration and an increase in ventilation rate make the real-time digital twin therapy safer for the patient. While including patient feedback in the developed digital twin did not significantly change the digital twin's performance in pain relief.

#### 4. Outlook

In this study, several model simplifications were considered for drug uptake, pharmacokinetics, and pharmacodynamics modeling. Not all processes that happen in the human body are exactly captured as in reality. Nevertheless, the models were validated and showed a good agreement with experimental data. Besides these assumptions, it is important to develop the digital twin based on real humans and connect the digital twin to the real patient by real-time sensor data or patient feedback. In order to obtain a more accurate digital twin to assist in the treatment, we should consider other factors. Here are some of the important model improvements that should be applied:

- In this study, the skin's geometry was a simple layered structure with no heterogeneity, and perfect contact between the patch and the surface of the skin was assumed. Developing a real structure of the skin by considering its geometry and different diffusion paths and

skin components will lead to a more accurate drug flux from the skin. However, it should be considered that the skin structure is very complex and differs depending on its location and the individual. If the modeling goes to a high level of individualization, every person and location must be measured, as literature data will be invalid. This may create new problems with the relevance and reliability of the measurement method. Therefore, a balance has to be found between the individualization/realism of the model and its practicability in order not to create new model artifacts that are greater than for a simplified model due to unreliable measurements of individual skin parameters.

- Advection – which is an important mechanism in drug penetration – could be included by considering the dermis' capillary vessels. In this study, the capillary network was not considered explicitly but accounted for in the model through an equivalent diffusion length of the dermis.
- As mentioned in the sensitivity analysis section ([Supplementary material](#)), the fraction of unbound drug has an important role in the plasma's calculated fentanyl concentration. In our model, a constant value was considered based on the literature. Considering its reaction's kinetics would lead to different values as a function of time and concentration for each patient, which will increase the accuracy of the digital twin.
- An important issue in opioid therapy is the changing opioid tolerance of the patient through the use of opioids over time. Increasing this tolerance will increase the required drug for pain relief; therefore, it could be considered in the model.
- Here we only controlled therapy, so the changing of the patches, based on the pain level of the patient. Reducing the adverse effects is crucial to reach an effective and safe treatment; it is important to control therapy based on therapeutic effects and adverse effects.
- Besides the impact of age between different patients, also other factors need to be considered. Physiological features of the patients, such as gender, weight, or background disease, can play an important role in the outcome of fentanyl therapy.
- To analyze the digital twin's performance in providing efficient and safe treatment, it is important to develop a digital twin based on the real patient. In this case, the twin can be updated with patient feedback over time. The result of the digital twin precalibrated therapy can then be compared with the real result to validate each individual patient's digital twin's performance. It should be noted that the assessment of the parameters of the real patient may introduce new errors due to the accuracy and reliability of the used sensors.
- In this study, the fentanyl patch was modeled based on a Duragesic® fentanyl transdermal system. In the future, considering more varied patch types will broaden the possibilities to tailor therapy for the patient. For some patches, this includes taking into account a more detailed model of the patch, with different layers and their

properties, plus the adherence of the patch to the skin. In future simulations, the impact of external factors such as ambient temperature on drug diffusion can also be accounted for. In the model, this would imply changing the diffusion coefficient of fentanyl.

- During the fentanyl transdermal therapy, the patient might take other pain medicines that can affect the fentanyl therapy. These medicines should also be added to the PK and PD models.
- Patients undergoing fentanyl transdermal therapy may have other diseases or organ impairments. These conditions may affect the drug uptake, drug distribution, metabolism, elimination, or drug effects. In a future step, it is essential to consider these conditions to reach a tailored treatment for the patients.
- Each individual patient is different from one another due to the lifestyle, genetic variation, and surrounding environment. These differences will lead to the variation in their response to fentanyl transdermal therapy. In order to reach a tailored therapy that is compatible with the patient, these factors must be included in the future. In this study, as we studied one individual patient, we assumed the only changing factor for the patient is age.

## 5. Conclusions

In this study, we developed a physics-based digital twin for fentanyl transdermal therapy. With this twin, we first anticipated the outcome of conventional transdermal therapy on a patient of different ages. In addition, based on the age of the patient and the corresponding response of the patient to treatment, the digital twin was used to propose a predefined alternative transdermal therapy for the patient at each age, namely by changing the patches at a different time interval. Finally, the proposed therapy by digital twin was updated by virtual patient feedback to have a more accurate and safer therapy.

Based on the result of the simulation by aging, the patient will receive a lower amount of drug as a result of the increase in the thickness of the stratum corneum for conventional therapy that is now used in the clinics. However, as the required amount of drug for pain relief decreases by age, older patients still experience more pain relief, despite a lower blood concentration. By applying conventional therapy, younger patients had a maximum fentanyl flux out of the dermis that was 11% higher, the maximum concentration of fentanyl that was 7% higher, and pain relief that was 55% lower than older patients. When the digital twin proposed a different therapy for each age category, younger patients needed to apply patches more frequently compared to the older patient to reach the target pain relief. This twin-assisted therapy reduced the VAS pain score by 30% and the time without pain increased by 314% for a patient at the age of 20 years, compared to conventional therapy. In the next step, the digital twin included patient feedback on their pain intensity at certain times. With such feedback, the therapy was better tailored to real-time patients' needs and avoided delivering insufficient or extra fentanyl. By including

the patient's feedback in the digital twin, we successfully were able to avoid hypoventilation, which means the therapy was safer for the patient.

The proposed physics-based digital twin was built up based on the real patient's physiological features. The digital twin was able to monitor the concentration of fentanyl in every organ throughout the therapy in parallel to the pain intensity of the patient and the breathing rate. Throughout the therapy, the digital twin updated itself via patient feedback. By considering the intensive monitoring of twins on the patient and therapy, the twin was able to propose a therapy based on the patient's needs. The proposed therapies by a digital twin for the patient can increase the concentration of the drug at a level to reach the required pain relief while avoiding its adverse effects. We quantified the added value of a patient's physics-based digital twins and sketched the future roadmap for implementing such twin-assisted treatment into the clinics.

## Author contributions

TD and RR conceptualized the study and acquired funding. TD did the project administration. FB performed the investigation, developed the methodology, performed the validation, and executed the simulations. TD supervised FB. FB wrote the original draft of the paper and did the visualization. TD and RR performed critical reviews and editing.

## Disclosure statement

The authors declare no competing interest.

## Funding

This work was financially supported by the Novartis Research Foundation (grant "Virtual twinning for intelligent, personalized transdermal drug delivery"). The funder (Novartis Research Foundation) was not involved in the study design, collection, analysis, and interpretation of data, the writing of this article, or the decision to submit it for publication.

## Data availability statement

The supporting raw data of this article will be made accessible by the authors without undue reservation.

## References

- Algera MH, Kamp J, van der Schrier R, et al. (2019). Opioid-induced respiratory depression in humans: a review of pharmacokinetic-pharmacodynamic modelling of reversal. *Br J Anaesth* 122:e168–e179.
- Andresen T, Upton RN, Foster DJR, et al. (2011). Pharmacokinetic/pharmacodynamic relationships of transdermal buprenorphine and fentanyl in experimental human pain models. *Basic Clin Pharmacol Toxicol* 108:274–84.
- Anissimov YG, Jepps OG, Dancik Y, Roberts MS. (2013). Mathematical and pharmacokinetic modelling of epidermal and dermal transport processes. *Adv Drug Deliv Rev* 65:169–90.
- Berner B, John VA. (1994). Pharmacokinetic characterisation of transdermal delivery systems. *Clin Pharmacokinet* 26:121–34.
- Bjorkman S, Wada RD, Stanski D. (1998). Application of physiologic models to predict the influence of changes in body composition and

- blood flows on the pharmacokinetics of fentanyl and alfentanil in patients. *Anesthesiology* 88:657–67.
- Björkman S. (2003). Reduction and lumping of physiologically based pharmacokinetic models: prediction of the disposition of fentanyl and pethidine in humans by successively simplified models. *J Pharmacokinetic Pharmacodyn* 30:285–307.
- Boireau-Adamezyk E, Baillet-Guffroy A, Stamatas GN. (2014). Age-dependent changes in stratum corneum barrier function. *Skin Res Technol* 20:409–15.
- Breitbart W, Chandler S, Egel B. (2000). An alternative algorithm for dosing transdermal fentanyl for cancer-related pain. *Oncology* 14: 695–705.
- Caraceni A, Hanks G, Kaasa S. (2012). Use of opioid analgesics in the treatment of cancer pain: evidence-based recommendations from the EAPC. *Lancet Oncol* 13:58–68.
- Casey M, Wintergerste T. (2000). Special interest group on “quality and trust in industrial CFD” best practice guidelines, First edit. ERCOFTAC: European Research Community on Flow Turbulence and Combustion 2000.
- Chaves C, Remiao F, Cisternino S, Decleves X. (2017). Opioids and the blood-brain barrier: a dynamic interaction with consequences on drug disposition in brain. *Curr Neuropharmacol* 15:1156–73.
- Chen J, Jiang QD, Chai YP, et al. (2016). Natural terpenes as penetration enhancers for transdermal drug delivery. *Molecules* 21:1709–22.
- Chien YW, Lin S. (2007). Drug delivery: controlled release. In *Encyclopedia of Pharmaceutical Technology*, Third Edit., J. Swarbrick, Ed. New York: Informa Healthcare, p. 2092.
- Corral-Acero J, Margara F, Marciniak M, et al. (2020). The ‘Digital Twin’ to enable the vision of precision cardiology. *Eur Heart J* 41:4556–64.
- Defraeye T, Shrivastava C, Berry T, et al. (2021). Digital twins are coming: Will we need them in supply chains of fresh horticultural produce? *Trends in Food Science & Technology* 109:245–58.
- Defraeye T, Bahrami F, Ding L, et al. (2020). Predicting transdermal fentanyl delivery using mechanistic simulations for tailored therapy. *Front Pharmacol* 11:1487.
- Defraeye T, Bahrami F, Rossi RM. (2021). Inverse mechanistic modeling of transdermal drug delivery for fast identification of optimal model parameters. *Front Pharmacol* 12:442.
- Dequidt J, Courtecuisse H, Comas O, et al. (2013). Computer-based training system for cataract surgery. *Simulation* 89:1421–35.
- Encinas E, Calvo R, Lukas JC, et al. (2013). A predictive pharmacokinetic/pharmacodynamic model of fentanyl for analgesia/sedation in neonates based on a semi-physiologic approach. *Paediatr Drugs* 15: 247–57.
- FDA. (2016). Reporting of Computational Modeling Studies in Medical Device Submissions – Guidance for Industry and Food and Drug Administration Staff.
- Feng Y, Chen X, Zhao J. (2018). Create the individualized digital twin for noninvasive precise pulmonary healthcare. *Significances Bioeng Biosci* 1.
- Feng Y, Zhao J, Kleinstreuer C, et al. (2018). An in silico inter-subject variability study of extra-thoracic morphology effects on inhaled particle transport and deposition. *J Aerosol Sci* 123:185–207.
- Geist MJP, Ziesenitz VC, Bardenheuer HJ, et al. (2019). Minor contribution of cytochrome P450 3A activity on fentanyl exposure in palliative care cancer patients. *Sci Rep* 9:6–11.
- Grond S, Radbruch L, Lehmann KA. (2000). Clinical pharmacokinetics of transdermal opioids: focus on transdermal fentanyl. *Clin Pharmacokinetic* 38:59–89.
- Gupta R, Rai B. (2018). In-silico design of nanoparticles for transdermal drug delivery application. *Nanoscale* 10:4940–51.
- Heikkinen EM, Voipio H-M, Laaksonen S, et al. (2015). Fentanyl pharmacokinetics in pregnant sheep after intravenous and transdermal administration to the ewe. *Basic Clin Pharmacol Toxicol* 117:156–63.
- Hill R, Santhakumar R, Henderson G, et al. (2020). Fentanyl depression of respiration: comparison with heroin and morphine. *Br J Pharmacol* 177:254–65.
- Jeal W, Benfield P. (1997). Transdermal fentanyl. A review of its pharmacological properties and therapeutic efficacy in pain control. *Drugs* 53:109–38.
- Karin Homber JH, Kong J, Lee S. (2008). The effects of applied local heat on transdermal drug delivery systems.
- Kuip EJM, Oldenmenger WH, Visser-Thijs MF, et al. (2018). Influence of aprepitant and localization of the patch on fentanyl exposure in patients with cancer using transdermal fentanyl. *Oncotarget* 9: 18269–76.
- Kuip EJM, Zandvliet ML, Koolen SLW, et al. (2017). A review of factors explaining variability in fentanyl pharmacokinetics; focus on implications for cancer patients. *Br J Clin Pharmacol* 83:294–313.
- Lennernäs B, Hedner T, Holmberg M, et al. (2005). Pharmacokinetics and tolerability of different doses of fentanyl following sublingual administration of a rapidly dissolving tablet to cancer patients: a new approach to treatment of incident pain. *Br J Clin Pharmacol* 59:249–53.
- Li J, Yan K, Hou L, et al. (2017). An algorithm and R program for fitting and simulation of pharmacokinetic and pharmacodynamic data. *Eur J Drug Metab Pharmacokinetic* 42:499–518.
- Lundborg M, Wennberg CL, Narangifard A, et al. (2018). Predicting drug permeability through skin using molecular dynamics simulation. *J Control Release* 283:269–79.
- Macintyre PE, Jarvis DA. (1996). Age is the best predictor of postoperative morphine requirements. *Pain* 64:357–64.
- Madden JC, Pawar G, Cronin MTD, et al. (2019). In silico resources to assist in the development and evaluation of physiologically-based kinetic models. *Comput. Toxicol* 11:33–49.
- Manitz R, Lucht W, Strehmel K, et al. (1998). On mathematical modeling of dermal and transdermal drug delivery. *J Pharm Sci* 87:873–9.
- Marier JF, Lor M, Potvin D, et al. (2006). Pharmacokinetics, tolerability, and performance of a novel matrix transdermal delivery system of fentanyl relative to the commercially available reservoir formulation in healthy subjects. *J Clin Pharmacol* 46:642–53.
- Miller RS, Peterson GM, McLean S, Möller C. (1997). Effect of cardiopulmonary bypass on the plasma concentrations of fentanyl and alcuronium. *J Clin Pharm Ther* 22:197–205.
- Muijsers RBR, Wagstaff AJ. (2001). Transdermal fentanyl: an updated review of its pharmacological properties and therapeutic efficacy in chronic cancer pain control. *Drugs* 61:2289–307.
- Naegel A, Heisig M, Wittum G. (2013). Detailed modeling of skin penetration—an overview. *Adv Drug Deliv Rev* 65:191–207.
- Nelson L, Schwaner R. (2009). Transdermal fentanyl: pharmacology and toxicology. *J Med Toxicol* 5:230–41.
- Obara S, Egan TD. (2013). Pharmacokinetic and pharmacodynamic principles for intravenous anesthetics. Second Edi. Elsevier Inc.
- Olkkola KT, Palkama VJ, Neuvonen PJ. (1999). Ritonavir’s role in reducing fentanyl clearance and prolonging its half-life. *The Journal of the American Society of Anesthesiologists* 91:681–685.
- Orsini JA, Moate PJ, Kuersten K, et al. (2006). Pharmacokinetics of fentanyl delivered transdermally in healthy adult horses—variability among horses and its clinical implications. *J Vet Pharmacol Ther* 29:539–46.
- Pan S, Duffull SB. (2019). Automated proper lumping for simplification of linear physiologically based pharmacokinetic systems. *J Pharmacokinetic Pharmacodyn* 46:361–70.
- Paut O, Camboulives J, Viard L, et al. (2000). Pharmacokinetics of transdermal fentanyl in the peri-operative period in young children. *Anaesthesia* 55:1202–7.
- Ramos-Matos CF, Lopez-Ojeda W. (2017). Fentanyl. In: StatPearls [Internet]. Treasure Island (FL): StatPearls Publishing.
- Rees WD. (1990). clinical oncology opioid needs of terminal care patients: variations with age and primary site. *Clin Oncol* 2:79–83.
- Rim JE, Pinsky PM, Van Osdol WW. (2005). Finite element modeling of coupled diffusion with partitioning in transdermal drug delivery. *Ann Biomed Eng* 33:1422–38.
- Robert L, Robert A. (2009). Physiologie du vieillissement cutané. *Pathologie Biologie* 57:336–341.
- Ruan J, Wan X, Quan P, et al. (2019). Investigation of effect of isopropyl palmitate on drug release from transdermal patch and molecular dynamics study. *AAPS PharmSciTech* 20:1–12.
- Sandler AN, Stringer D, Panos L, et al. (1992). A randomized, double-blind comparison of lumbar epidural and intravenous fentanyl infusions for postthoracotomy pain relief. Analgesic, pharmacokinetic, and respiratory effects. *Anesthesiology* 77:626–34.

- Schulz M, Schmoltdt A. (2003). Therapeutic and toxic blood concentrations of more than 800 drugs and other xenobiotics. *Pharmazie* 58: 447–74.
- Scott JC, Stanski DR. (1987). Decreased fentanyl and alfentanil dose requirements with age. A simultaneous pharmacokinetic and pharmacodynamic evaluation. *J Pharmacol Exp Ther* 240:159–66.
- Serlin RC, Mendoza TR, Nakamura Y, et al. (1995). When is cancer pain mild, moderate or severe? Grading pain severity by its interference with function. *Pain* 61:277–84.
- Sinisi S, Alimguzhin V, Mancini T. (2020). "Systems biology Complete populations of virtual patients for in silico clinical trials," vol. 36, pp. 5465–5472.
- Thompson JP, Bower S, Liddle AM, Rowbotham DJ. (1998). Perioperative pharmacokinetics of transdermal fentanyl in elderly and young adult patients. *Br J Anaesth* 81:152–4.
- Upton RN, Foster DJR, Abuhelwa AY. (2016). An introduction to physiologically-based pharmacokinetic models. *Paediatr Anaesth* 26:1036–46.
- US Food and Drug Administration, "Duragesic Label". (2005).
- Van der Paal J, Fridman G, Bogaerts A. (2019). Ceramide cross-linking leads to pore formation: potential mechanism behind CAP enhancement of transdermal drug delivery. *Plasma Process. Polym* 16:1–10.
- Walicka A, Iwanowska-Chomiak B. (2018). Drug diffusion transport through human skin. *Int J Appl Mech Eng* 23:977–88.
- Weiser JR, Saltzman WM. (2014). Controlled release for local delivery of drugs: barriers and models. *J Control Release* 190:664–73.
- Woodhouse A, Mather LE. (1997). The influence of age upon opioid analgesic use in the patient-controlled analgesia (PCA) environment. *Anaesthesia* 52:949–55.
- Wright DFB, Winter HR, Duffull SB. (2011). Understanding the time course of pharmacological effect: a PKPD approach. *Br J Clin Pharmacol* 71:815–23.
- Yang D, Wan X, Quan P, et al. (2018). The role of carboxyl group of pressure sensitive adhesive in controlled release of propranolol in transdermal patch: quantitative determination of ionic interaction and molecular mechanism characterization. *Eur J Pharm Sci* 115:330–8.
- Yassen A, Olofsen E, Kan J, et al. (2008). Pharmacokinetic-pharmacodynamic modeling of the effectiveness and safety of buprenorphine and fentanyl in rats. *Pharm Res* 25:183–93.
- Yassen A, Olofsen E, Romberg R, et al. (2007). Mechanism-based PK/PD modeling of the respiratory depressant effect of buprenorphine and fentanyl in healthy volunteers. *Clin Pharmacol Ther* 81:50–8.